CORA Cork Open Research Archive
Cartlann Taighde Oscailte Chorcaí

UCC Library and UCC researchers have made this item openly available. Please let us know how this has helped you. Thanks!

Title	An assessment of sputtered nitrogen-doped nickel oxide for all-oxide transparent optoelectronic applications: The case of hybrid NiO:N/TiO2 heterostructure
Author(s)	Aivalioti, Chrysa; Papadakis, Alexandros; Manidakis, Emmanouil; Kayambaki, Maria; Androulidaki, Maria; Tsagaraki, Katerina; Pelekanos, Nikolaos T.; Stoumpos, Constantinos; Modreanu, Mircea; Crăciun, Gabriel; Romanitan, Cosmin; Aperathitis, Elias
Publication date	2022-02-12
Original citation	Aivalioti, C., Papadakis, A., Manidakis, E., Kayambaki, M., Androulidaki, M., Tsagaraki, K., Pelekanos, N. T., Stoumpos, C., Modreanu, M., Crăciun, G., Romanitan, C. and Aperathitis, E. (2022) 'An assessment of sputtered nitrogen-doped nickel oxide for all-oxide transparent optoelectronic applications: The case of hybrid NiO:N/TiO2 heterostructure', in Recent Trends in Chemical and Material Sciences Vol. 6. London: B P International, pp. 86-111. doi: 10.9734/bpi/rtcams/v6/1650A
Type of publication	Book chapter
Link to publisher's version	http://dx.doi.org/10.9734/bpi/rtcams/v6/1650A Access to the full text of the published version may require a subscription.
Rights	**© 2022, the Authors. This is an open access chapter distributed under the Creative Commons Attribution License which permits unrestricted use, distribution, and reproduction in any medium, provided the original work is properly cited.** https://creativecommons.org/licenses/by/4.0/
Item downloaded from	http://hdl.handle.net/10468/12645

Downloaded on 2022-05-18T19:43:33Z

UCC
University College Cork, Ireland
Coláiste na hOllscoile Corcaigh

Print ISBN: 978-93-5547-050-8, eBook ISBN: 978-93-5547-058-4

An Assessment of Sputtered Nitrogen-Doped Nickel Oxide for all-Oxide Transparent Optoelectronic Applications: The Case of Hybrid NiO:N/TiO_2 Heterostructure

Chrysa Aivalioti [a,b], Alexandros Papadakis [c], Emmanouil Manidakis [a,b], Maria Kayambaki [b], Maria Androulidaki [b], Katerina Tsagaraki [b], Nikolaos T. Pelekanos [a,b], Constantinos Stoumpos [a], Mircea Modreanu [d], Gabriel Crăciun [e], Cosmin Romanitan [e] and Elias Aperathitis [b*]

DOI: 10.9734/bpi/rtcams/v6/1650A

ABSTRACT

Transition metal oxides present a unique category of materials due to their versatile optical, electrical and mechanical properties. Nickel oxide (NiO) is an intrinsic p-type oxide semiconductor. P-NiO with controllable and reproducible physico-chemical properties, if combined with transparency and low temperature (low-T) fabrication processes, can be fully exploited in many transparent and/or flexible devices for applications, like energy management (production, manipulation, storage), sensing, wearable and health care electronics, etc. Reproducibility, transparency and low-T fabrication processes of p-type NiO are the motivation of this work. Nitrogen is one of the dopants used for modifying the properties of NiO. Until now, nitrogen-doped NiO, has shown inferior properties than those of pure NiO. In this work, we present nitrogen-doped NiO (NiO:N) thin films with enhanced properties compared to those of the undoped NiO. The NiO:N films were grown by sputtering on room-temperature substrates in plasma containing 50% Ar and 50% (O_2+N_2) gases. The undoped NiO film was oxygen-rich, single-phase cubic NiO, having transmittance less than 20%. Upon doping with nitrogen, the films became more transparent (around 65%), had a wide direct band gap (up to 3.67 eV) and showed clear evidence of indirect band gap, 2.50-2.72 eV, depending on %(O_2-N_2) in plasma. The changes in the properties of the films such as structural disorder, energy band gap, Urbach states and resistivity were correlated with the incorporation of nitrogen in their structure. The optimum NiO:N film was used to form a diode with spin-coated, mesoporous on top of a compact, TiO_2 film. The hybrid NiO:N/TiO_2 heterojunction was transparent showing good output characteristics, as deduced using both I-V and Cheung's methods. The diode's transparency and characteristics were further enhanced upon thermal treatment and this was attributed to improved NiO:N properties with annealing. Transparent NiO:N films can be realized for all-oxide flexible optoelectronic devices.

Keywords: NiO; N-doped NiO; Urbach tail; sputtering; mesoporous TiO_2; spin-coating; NiO:N/TiO_2 heterojunction; optical properties; diode properties.

1. INTRODUCTION

Nickel oxide (NiO) is considered the prototype p-type oxide semiconductor [1,2] and combined with the reported values of its energy band gap in the range of 3.6-4.0 eV it is the most widely used p-type

---

[a] Department of Materials Science and Technology, University of Crete, P.O. Box 2208, 71003, Heraklion, Crete, Greece.
[b] Microelectronics Research Group, Institute of Electronic Structure and Laser, Foundation for Research and Technology (FORTH-Hellas), P.O. Box 1385, Heraklion, Greece.
[c] Department of Physics, University of Crete, P.O. Box 2208, 71003, Heraklion, Crete, Greece.
[d] Tyndall National Institute-University College Cork, Lee Maltings, Dyke Parade, Cork, T12 R5CP, Ireland.
[e] National Institute for Research and Development in Microtechnologies -IMT, Bucharest, Romania.
**Corresponding author: E-mail: eaper@physics.uoc.gr;*

transparent conductive oxide. Due to its chemical stability and non-toxicity, NiO has found numerous applications in photo-bio-catalysis [3-5], sensing [6-8], microbatteries [9] and transparent optoelectronics such as smart windows [10], ultra-violet (UV) photodetectors [11] and photovoltaics (PVs). In the case of PVs, NiO has been used in conventional PVs and ultra-violet UV-PVs [12-14] in addition to perovskite PVs in which it is used as hole transport layer [15-17]. If NiO is to be used for applications in which it can be applied as a coating or single layer, relatively low-cost chemical methods are generally employed for its fabrication, like sol-gel and spray pyrolysis. However, when p/n junctions and well-defined and controllable geometries are required for oxide-based optoelectronic applications then dry (solid-state) methods are used as the physical vapor deposition technique of sputtering. In addition, the formation of the oxide on unintentionally heated substrates is pursued if applications in the emerging and challenging field of flexible, foldable and stretchable optoelectronics (PVs, wearables, etc) are sought. Low temperature depositions (<200°C) promote the growth of semi-transparent and non-stoichiometric NiO [18-21]. Ab initio calculations, based on combinatorial modeling approaches for predicting details of the electronic band structure of NiO and thus values for its band gap and charge transport properties even down to the nanoscale [1,22,23] generally yield underestimated values when compared to experimentally extracted values. Regardless of the method of fabrication, the growth-induced gap states, such as intermediate sub-gap states, Urbach tails and non-stoichiometry, play an important role in the optical and electrical properties of the material.

Stoichiometric NiO is an insulator and the p-type conductivity arises due to intrinsic defects such as interstitial oxygen (I_O) and/or nickel vacancies (V_{Ni}) especially when grown in oxygen-rich deposition conditions in which non-stoichiometric growth of NiO is promoted. According to the proposed reaction [19,24]: $2Ni^{2+} + 1/2O_2 \rightarrow 2Ni^{3+} + I_O + 2V_{Ni}$, two Ni^{2+} ions react with oxygen and produce interstitial oxygen, two V_{Ni} ionized defects and two Ni^{3+} ions, contributing thus to extra holes to the system. However, the holes are strongly localized giving rise to rather low hole mobilities (<0.1 cm^2/Vs) and, because the V_{Ni} transition levels are not shallow enough, the concentration of free-holes is rather low (<10^{15} cm^{-3}) [1,13,25]. Nevertheless, NiO has been investigated as a p-type layer in p/n junctions for all-oxide optoelectronic applications, where the n-type layer for forming the heterostructure has been TiO_2 [14,26], ZnO [27,28], Ga_2O_3 [29], Nb_2O_5 [6], InN [30], SnO_2 [31], etc. Due to the versatile and technological importance of NiO material design concepts have been proposed, such as the substitutional cation and/or anion doping of NiO, to modify its properties depending on the application. Thus, doping of NiO with single dopants such as Al [32], Li [33], Cu [34], Nb [35], N [36-40] or co-doping like Li-Al [41], Li-Mg [42] and Cu-N [43], has been reported. As in the case where low-temperature depositions are performed, it is generally agreed that different dopants can lead to different structural distortions, which in turn have significant effects on the electronic structure, defect levels and consequently on the properties of the material [44].

Table 1. Literature reports on NiO:N thin films properties: Depos. Techn. = deposition technique, T_{sub} = substrate's temperature, d = thickness, TT = thermal treatment, T_{VIS} = visible transmittance, E_{gap} = energy band gap, RF MS = radio frequency magnetron sputtering, DC MS = direct current magnetron sputtering, RF S = radio frequency sputtering

Depos. Techn.	T_{sub} (^{o}C)	d (nm)	TT	Optical Properties	T_{VIS} / E_{gap} direct (E_{gap} indirect)	Resistivity or resistance	Ref.
Chemical	280	10	-	NiO	-	7.1 MΩcm	[38]
solution				NiO:N	80-82% / -	4.8 MΩcm	
Sol-gel	120	200	450°C	NiO	~70% / 4eV (3.5eV)	-	[36]
			1 h	NiO:N	50-70% / 3.8eV (3.25eV)	-	
Spray	350	720-900		NiO	~40-60% / 3.5eV (3.41eV)	3.8 kΩcm	[37]
techn.				NiO:N	30-50% / 3.45eV	1.7 kΩcm	
RF MS	100-400	300	-	NiO	~90% / 3.53eV	28.3 Ω	
				NiO:N	90% / 3.5eV	28 Ω	[39]
DC MS	RT	300		NiO:	~30-40% / 3.6eV	-	[35]
				NiO:N	<40% / 3.3eV (2.3eV)	-	
RF S	RT	~150		NiO	~7% / 3.15eV	23 kΩ	This
				NiO:N	45-70% / 3.67eV (2.72eV)	>100 kΩ	work

Almost ten years ago, in an attempt to predict band gap modulation via theoretical calculations [22], it was revealed that the wide band gap of NiO could be narrowed by nitrogen doping (NiO:N). Since then, NiO:N thin films have been made by wet methods [37-39] or dry methods (rf or dc sputtering) [36,40] and the main properties of these undoped and N-doped NiO films are tabulated in Table 1. It is seen that in most cases heated substrates are used and the introduction of nitrogen to the NiO structure has resulted in films with reduced transmittance and resistivity compared to undoped NiO films. Furthermore, in most reports of Table 1, both undoped and N-doped NiO were treated as materials having direct and indirect band gaps.

In this work, we fabricated NiO:N thin films by rf sputtering on unintentionally heated substrates, examined their physical properties and applied the transparent p-NiO:N on n-type TiO_2 layers. The n-TiO_2 layers were those used as electron transfer layers for perovskite solar cells (mesoporous TiO_2 on top of a compact TiO_2) made by the spin-coating technique. It is worth mentioning that mesoporous TiO_2 has been reported in the literature for the formation of all-organic NiO/TiO_2 heterostructure for photocatalytic and biosensing applications [45,46]. The formed hybrid NiO:N/TiO_2 heterostructures were tested for their output characteristics just after formation and after thermal treatment. Nitrogen-doped NiO films were found to be highly transparent, rendering NiO:N films as potential candidates for transparent electronic and photonic applications. Potential improvements and modifications of the fabrication procedure of the hybrid NiO:N/TiO_2 heterojunction are also addressed.

2. MATERIALS AND METHODS

2.1 Thin Films Deposition

2.1.1 NiO Films preparation

Nitrogen-doped NiO films, and an undoped NiO film as a reference, were fabricated by RF sputtering (Nordiko NS2500) using a 6 in. diameter nickel (Ni) target (purity 99.99%) in plasma containing Ar-O_2-N_2 and Ar-O_2 gases, respectively (purities: Ar 99.999%, O_2 99.95% and N_2 99.999%). All films were deposited on unintentionally heated Si (100) wafer pieces and fused silica glass substrates, which were mounted 10 cm above the sputtering target. The glass substrates were ultrasonically cleaned in acetone and isopropanol, rinsed with deionized water and dried in the flow of nitrogen gas, whereas the Si substrates were dipped in 10% HF solution for 30 seconds to remove the native oxide from its surface before placing them into the sputtering chamber. Prior to depositions, the target was pre-sputtered for at least 20 min (Ar plasma, 5 mTorr, 300 W RF power) to remove any contaminants from the target surface and to enable equilibrium conditions to be reached. During deposition the RF power was set at 300 W and the total pressure was kept at 5 mTorr while the percentage of gases in plasma were adjusted by the ratio of their flow rates through a set of mass flow controllers. The plasma gases for the reference undoped NiO film (P0) were Ar:O_2=50:50. The nitrogen-containing films (P1, P2, P3) were made in plasma containing 50% Ar, as the reference NiO film P0, but O_2 was gradually substituted by N_2 keeping the sum of their flow rates percentage equal to 50 (%O_2+%N_2=50%) as follows: film P1: 50% Ar + (40% O_2 +10% N_2), film P2: 50% Ar + (25% O_2 +25% N_2) and film P3: 50% Ar + (10% O_2 +40% N_2). Furthermore, to verify the effect of Ar gas on the films' properties, one more film was grown in plasma containing much less Ar than that of films P1-P3 and consequently more %(O_2+N_2) gases, namely film P4: 6% Ar + 47% O_2 + 47% N_2. The deposition parameters of the films and their thicknesses, as measured by a Veeco Dektak 150 profilometer, are listed in Table 2.

2.1.2 TiO_2 Films preparation

Compact and mesoporous TiO_2 films were fabricated by spin coating following the standard procedure used when these layers are to be used as electron transfer layers for perovskite PVs. According to the perovskite solar cell technology, a thin compact TiO_2 layer is used so to eliminate the contact of the perovskite layer with the Sn_2O_3:F (FTO) layer of the FTO-covered glass, which is used as the substrate. Above this, the mesoporous TiO_2 is used to increase the effective area of the perovskite-TiO_2 interface. More precisely, commercially available Sn_2O_3:F (FTO)-coated glass was used as substrate (600 nm and 2 mm thick, respectively), which were cleaned in a standard procedure: sonicated for 10 minutes in deionized water solution followed by an extra sonication step

in acetone and then in isopropanol for 10 minutes, rinsed with acetone and dried in N_2-gas flow. After the cleaning process and properly masking part of the FTO layer by vacuum tape mask, the TiO_2-containing solution was spin-coated (2000 rpm, 30s) on the FTO substrates. The solution was 50 μL of HCl (37%), 2.3 mL of ethanol and 150 μL of titanium isopropoxide, which was stirred for several hours. In this way, a compact TiO_2 (c-TiO_2) film, having a thickness of around 60 nm, was formed, which was followed by thermal treatment at 500 °C for 15min in ambient air. After the annealing of the c-TiO_2 layer, the substrates were plasma treated in oxygen and then a commercially available TiO_2mesoporous paste diluted in ethanol was spin-coated (6000rpm, 30s) on top of the c-TiO_2/FTO/glass substrate. The mesoporous TiO_2 (m-TiO_2) layer formed was around 200 nm thick and was afterward annealed at 500 °C for 15 min in air. The formed m-TiO_2/c-TiO_2/FTO/glass substrates were used for depositing the NiO layers.

2.2 Fabrication of NiO:N/TiO_2 Heterojunction

After preparing the m-TiO_2/c-TiO_2 layers as described above, the m-TiO_2/c-TiO_2/FTO/glass substrates were placed in the sputtering chamber. When the base-pressure was greater than 10^{-6}Torr the deposition conditions of NiO:N film P2 were applied (plasma containing flow rates percentage of $Ar:O_2:N_2$=50/25/25). The reason for choosing these plasma conditions is explained in the next sections. The device was completed by sputtering deposition of 150 nm thickness and 1 mm diameter Au as the ohmic contact on the NiO:N and FTO layers, using the appropriate shadow mask, which defined the junction area of the diode. A schematic representation of the fabricated NiO:N/TiO_2 heterodiodes can be seen in Fig. 1. The diodes were characterized just after fabrication and after thermal treatment (TT) in a glass tube furnace (Elite Thermal Systems Ltd) at different temperatures up to 500 °C for 15 min in flowing N_2, namely TT1 = 300 °C, TT2 = 400°C and TT3 = 500 °C.

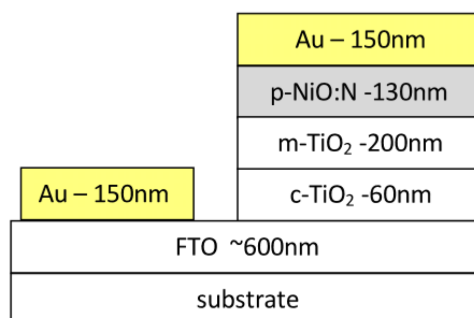

Fig. 1. Schematic representation of the fabricated NiO:N/TiO_2 heterodiode (NiO:N/m-TiO_2/c-TiO_2/FTO/glass). Thicknesses are not to scale

2.3 Thin Films and Device Characterization

Because the sputtering deposition of NiO films was performed on substrates that were not intentionally heated, photolithography was possible and a specially designed photolithography mask was used having the required patterns for the characterization of the films on an area of 1 x 1inch. Thus, all structural, optical and electrical properties of the sputtered films deposited on a single patterned square (1 x 1inch) glass substrate could be obtained. In this way, any possible non-uniformities and properties discrepancies between films from different deposition runs but the same deposition conditions were eliminated.

The crystallographic phases and crystallinity of the films were studied by the X-ray diffraction (XRD) method. The measurements were performed using a Bruker D8 ADVANCE XRD system employing a Cu KR source with Cu $K_{\alpha}1$ radiation (λ=1.5406 Å) and a power source of 40 kV and 40 mA. The films were scanned at grazing incidence (1.6°) and the collection angle extended from 20-90° with a rate of 0.02°/sec. The broadening and angle position of the most prominent peak in terms of diffraction intensity were used to determine the crystallite size and lattice strain in the films. The mean crystallite size was estimated from the Scherrer formula: $D = k\lambda/\beta_{hkl}\cos\theta$, where *k* is the shape factor 0.94, λ is

the wavelength of incident radiation 1.5406 Å, hkl represents the Muller indices of the diffracted plane, β_{hkl} is the full width at half maximum (FWHM), and θ is the Bragg angle of the peak. The lattice strain, which is also responsible for shifting the position of the diffraction peak, was determined using the formula: $\varepsilon_L = \beta_{hkl}\cot\theta/4$ [47].

Atomic force microscopy (AFM) measurements were performed in order to examine the surface morphology and roughness of the films. A Digital Instrument-Multimode system was employed, with resolution scanner of 100 μm × 100 μm × 5.6 μm working in the tapping mode by using sharp tips (radius of curvature of less than 10-15 nm) from Veeco.

Field-Emission Scanning Electron Microscope (FE-SEM) images were obtained using a Jeol JSM-7000F electron microscope equipped with an Energy-Dispersive X-ray (EDX) spectroscopy system (Oxford Instruments-INCA) for element analysis on the films.

X-ray photoemission spectroscopy (XPS) was performed on selected undoped and nitrogen-doped NiO films grown on Si to confirm and identify bonding of N in Ni-O structure. The XPS spectra were recorded on a Specs Lab photoelectron spectrometer using an Al Kα X-ray source at 13 kV and a power of 200 W. The analyzed area of the films' surface was 1.3×1.3 mm^2. The pressure in the analysis chamber was kept below $1x10^{-6}$ mTorr. Wide scan survey spectra were collected from -5 to 1400 eV (binding energy) with a constant energy of 160 eV. The high-resolution spectra of Ni 2p and N 1s core levels were recorded using a pass energy of 30 eV. All spectra were calibrated such that the adventitious carbon C 1s main peak is at 284.8 eV. The CasaXPS software was used for analysis and all spectra were fitted using a Shirley-type background and a Lorentzian Asymmetric peak-shape. Before the XPS measurements, the samples were heated to ~100 ^oC for 5 min and their surface was etched for 10 min by 0.75 keV Ar^+ with current density ~5 mA/cm^2 in order to remove any adsorbed contaminants which could originate from transferring the sample through ambient conditions.

The optical properties of the films were examined by recording the normal incidence transmittance (T) and near normal incidence reflectance (R) in the UV-Vis-NIR spectrum by employing a Perkin Elmer Lambda 950 system. The optical band gap of the films was estimated through the relation [48,49]:

$$T=\frac{(1-R)^2e^{-ad}}{1-R^2e^{-2ad}} \quad (1)$$

where d is the thickness of the films and α is the absorption coefficient. Equation (1) takes into account multiple reflections in the film but assumes the same reflectance at the air/film and film/substrate interfaces and zero-absorbance for the substrate. By solving Equation (1) for the absorption coefficient α as a function of the measured quantities T, R and d the following Equation (2) can be obtained:

$$\alpha = \frac{1}{d}\ln\left(\frac{(1-R)^2+\sqrt{(1-R)^4+4T^2R^2}}{2T}\right) \quad (2)$$

By applying the Tauc plot in $((\alpha hv)^n$-vs-hv), where h is the Planck constant, v is the frequency and n=2 for direct allowed transitions, n = 1/2 for indirect allowed transitions, n = 2/3 for direct not allowed transitions, and n = 1/3 for indirect not allowed transitions [48], the corresponding energy band gap could be extracted.

The resistivity of the films was determined by employing the conventional four-probe Van der Pauw technique on films deposited on a glass substrate, which had cross patterns and Au ohmic contacts (150 nm thick) deposited by electron gun evaporation. For selected films ac-modulated Hall effect measurements were performed in an attempt to determine the type and concentration of carriers. The current–voltage (I–V) characteristics of the heterodiodes were recorded using the Agilent 4200-SCS unit.

3. RESULTS AND DISCUSSION

3.1 Thin FILMS PROPERTIES

3.1.1 Properties of NiO and NiO:N thin films

NiO thin films: Undoped NiO was deposited as reference film at 300 W RF-power in 5 mTorr total pressure consisting of 50% Ar and 50% O_2 gases (50% Ar + 50% O_2). Under these oxygen-rich deposition conditions, NiO was oxygen-rich, atomic percentage (at.%) O/Ni~1.72 as revealed by EDX measurements, and previous experiments showed that it exhibits p-type behavior [7]. The XRD pattern of the NiO film deposited on Si substrate is shown in Fig. 2. The XRD pattern yielded one main diffraction peak at around 42.6^o and a second one with much smaller intensity at around 62°, which were identified as diffraction peaks arising from (200) and (220) crystallographic planes of the cubic NiO phase, respectively (Joint Committee of Powder Diffraction Standards (JCPDS) card No: 78-0429). The polycrystalline undoped O-rich NiO films had a (200) crystallite size of 5.2 nm, as deduced from the Scherrer equation. The disorder in the structure, caused by the low-temperature growth induced defects such as excess O and Ni vacancies, created tensile stress shifting the diffraction peaks to lower angles compared to the crystal NiO of the JCPDS card. The lattice strain was calculated to be ε_L=1.78x10^{-2}. The predominant growth of sputtered NiO films in the [200] direction is generally observed for films deposited both on heated [18,19] and unheated substrates [19]. The surface morphology and roughness of undoped NiO film P0 is seen in the SEM and AFM images of Fig. 2b,c, respectively. The grains of the as-prepared NiO film were up to 40 nm wide whereas the root mean square (RMS) roughness was calculated to be 2.9 nm. Furthermore, the disorder in the as-prepared NiO structure created scattering centers for the incident photons giving films with very low visible transparency (<10%) and a direct optical energy gap of around 3.15 eV. The transmittance and reflectance of the NiO film are shown in Fig. 2d. It is seen that the structural defects of the as-prepared NiO film created states in the band gap resulting in a low transmittance and a very slow rate of increase in absorption coefficient (also shown in Fig. 2d) as photons with increasing energy are impinging on the film surface. It has been reported that Ni^{+2} vacancies create Ni^{+3} and in association with the stress and the defects of the structure (interstitial oxygen, boundaries of small grains-crystallites) can be responsible for the low visible transmittance [20,21,40] and the relatively low energy band gap (3.15 eV) of undoped NiO [20]. The optical properties of undoped NiO are discussed in more details in conjunction with the properties of the nitrogen-containing NiO films in the next section.

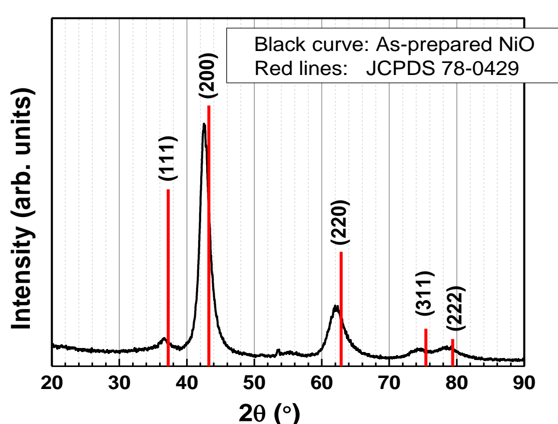

(a)

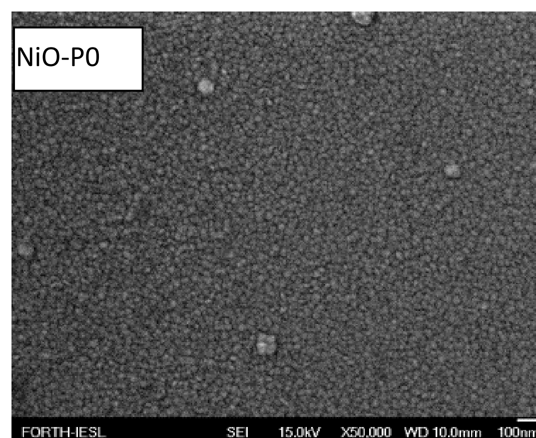

(b)

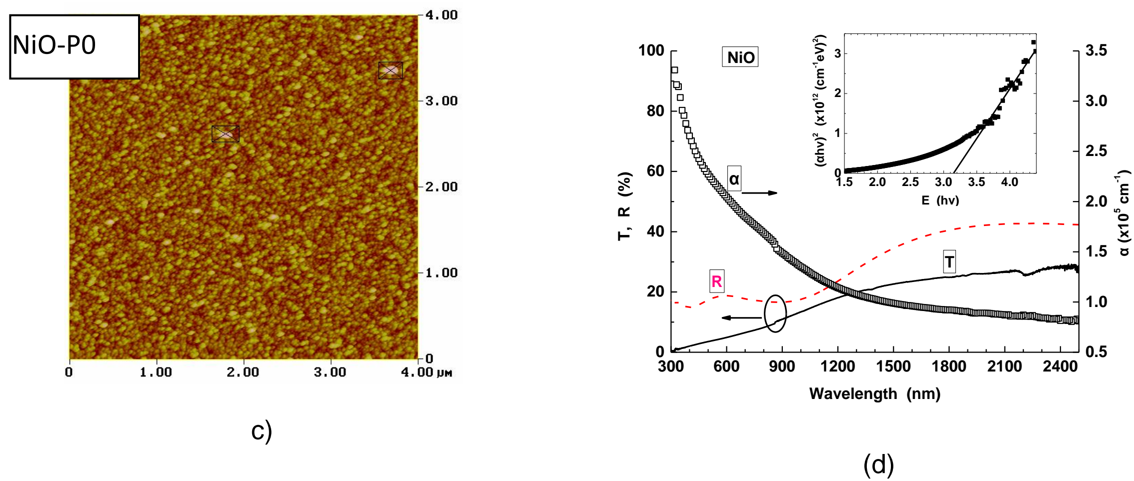

Fig. 2. (a) XRD pattern, (b) and (c) SEM and AFM images, respectively, and (d) UV-Vis-NIR transmittance, reflectance and absorption coefficient curves of NiO film (P0). The inset in (d) shows the $(\alpha hv)^2$-vs-E plot for deducing direct Egap

NiO:N thin Films: Nitrogen was introduced into the structure of NiO film P0 by performing depositions in plasma containing 50% Ar and 50% (O_2+N_2) gases as described in the Materials and Methods section. All nitrogen-doped and undoped NiO grown films, with their deposition conditions and properties, are tabulated in Table 2. Because the nitrogen atoms are lighter than the oxygen atoms, by gradually substituting O_2 by N_2 gas while keeping the %Ar in plasma constant, the deposition rate was reduced from 1.06 nm/min for films grown in N_2-free plasma (undoped NiO film P0) to 0.96 nm/min for 40% N_2 in plasma (NiO:N films P1 to P3 in Table 2). The deposition rate was further reduced to 0.64 nm/min when the deposition was performed in plasma containing only 6% Ar and 94% (O_2+N_2) -NiO:N film P4- as a result of the reduced sputtering yield caused by the heavier but fewer, in this case, inert argon atoms in plasma when compared to the O_2 and N_2 ones.

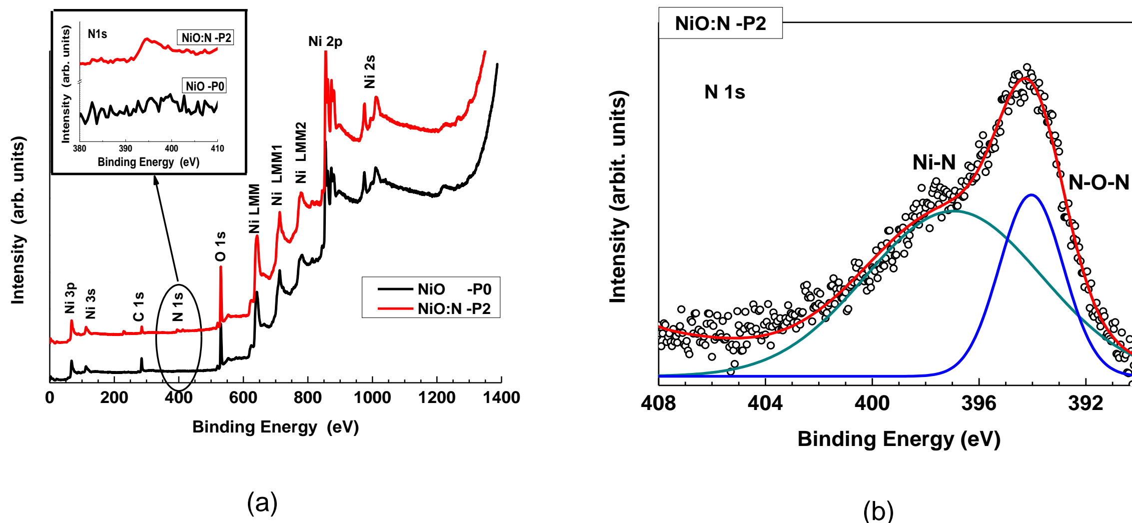

Fig. 3. (a) Wide-scan XPS spectra of undoped NiO (P0 film) and nitrogen doped NiO (P2 film). The inset shows expanded the location of N1s peak for both undoped and N-doped NiO. (b) High-resolution N1s core level spectra of nitrogen-doped NiO film (P2). Open cycles: experimental points, red line: superposition of the de-convoluted peaks (green and blue lines)

Table 2. Details of sputtering conditions and properties of undoped and N-doped NiO films. d = thickness, D.R. = Deposition Rate, D = crystallite size, ε_L = lattice strain, T = transmittance, Egap = energy gap, E_U = Urbach energy

Films		Deposition parameters					Structural properties			Optical properties			
		Flow rates (%)			d	D. R.	2θ	D	ε_L	T (%)	Direct Egap	Indirect Egap	E_U
		Ar	O_2	N_2	(nm)	(nm/min)	(degree)	(nm)	($x10^{-2}$)	(@550nm)	(eV)	(eV)	(meV)
NiO	**P0**	50	50	0	144	1.06	42.58	5.24	1.78	4.2	3.15	-	2,734
NiO:N	**P1**	50	40	10	128	1.52	42.65	6.15	1.20	51.7	3.65	2.56	933
	P2	50	25	25	133	1.05	42.71	9.14	1.15	49.1	3.67	2.72	592
	P3	50	10	40	159	0.94	42.70	6.69	1.32	29.3	3.59	2.50	830
	P4	6	47	47	142	0.64	42.64	7.16	1.39	51.2	3.65	2.74	598

Although the presence of nitrogen in Ni-O structure will be demonstrated in the next sections, by the different properties of undoped NiO and nitrogen-containing NiO films, initially EDX experiments were performed to quantify the amount of nitrogen in NiO films. However, although EDX results indicated that the atomic percentage (at.%) of nitrogen in the films increased as N_2 gas increased in plasma during deposition, the at.% of N was less than 1.5, regardless of the acceleration voltage for electrons in the EDX set-up (5 kV or 15 kV). Taking into account that EDX cannot accurately give the at.% of light atoms such as nitrogen and that values of at.% around or less than 1% are the limit of detection above the noise signal, XPS experiments were selectively performed for NiO:N -P2 film (50% Ar-25% O_2-25% N_2). It is worth noticing, however, that, as determined by EDX measurements, the at.% ratio of O/Ni of nitrogen-containing NiO films was around 5.2% less than that of undoped NiO (1.63 and 1.72, respectively).

Fig. 3a shows the wide-scan XPS spectra of undoped and nitrogen doped NiO, in which the characteristic peaks of Ni, O, N and C can be seen. Even though the mild Ar-ion sputtering of the surface which was performed in situ prior to the XPS experiment is known to cause preferential sputtering of species like oxygen and nitrogen [36,50], the nitrogen signal in XPS spectra could only be observed in the nitrogen-doped NiO film, unambiguously proving the presence of nitrogen in Ni-O structure. The incorporation of nitrogen into the NiO:N structure was examined in more detail by monitoring and de-convoluting the high resolution spectra of the N1s core level seen in Fig. 3b. The feature at 396.9 eV is attributed to nitrogen bound to Ni, whereas the second feature at 394.1 eV is believed to be associated with Ni-O-N [35,38,49]. The N concentration for NiO:N –P2 film was estimated to be 2.9 at.%.

The introduction of nitrogen in the structure of NiO films during growth did not affect its crystallographic cubic phase, as seen in Fig. 4a in which the XRD patterns of NiO:N films P1-P4 are presented. The films remained single-phase NiO films with no evidence of any other nickel oxide or nitride phases (Ni_2O_3, Ni_xN_y, etc). As tabulated in Table 2, upon nitrogen doping the (200) diffraction peak shifted to higher angles (approaching that of crystal NiO at 43.28°, JCPDS card No: 78-0429), the crystallite size increased by almost a factor of 2 and the lattice strain was reduced by 35% when compared to the respective properties of the undoped NiO. These changes were more profound for film P2, which was grown in plasma containing 50% Ar and 50% of O_2+N_2 with equal flow rates (O_2:N_2=25:25). However, although the introduction of nitrogen in undoped NiO (film P0) improved its structural properties, these properties did not remain unaffected for film P4 of Table 2, which was made in Ar-deficient plasma containing only 6% Ar and 94% (O_2+N_2). It is apparent that under these reactive sputtering conditions the quality and quantity of plasma species lowered the optimum structural quality of P2 film because more strain was introduced in the structure.

The typical surface morphology of nitrogen-containing NiO films is seen in Fig. 4b in which the SEM images of NiO:N P2 and P4 films are seen. No apparent differences could be observed between the surface morphology of nitrogen-containing P1-P3 films. The differences in the surface appearance of film P4 with that of film P2 of Fig. 4b,c are attributed to the Ar-deficient conditions used for depositing P4 film. However, when compared to the surface morphology of undoped NiO (film P0) in Fig. 2b, the nitrogen-containing films exhibit bigger grain size and rougher surface. As revealed by the AFM measurements of NiO:N –P2 film its RMS roughness was 13.6% larger when compared to the undoped NiO –P0 film (3.3 nm versus 2.9 nm, respectively) but it was 60% smoother than Ni:O –P4 film (3.3 nm versus 5.3 nm, respectively). As seen in Table 2, the introduction of nitrogen in the structure of NiO shifted the diffraction peaks to higher angles, increased the crystallite size and reduced the lattice strain of undoped NiO. This indicated that the disordered undoped NiO structure became less disordered by the introduction of nitrogen in the lattice by reducing-filling of Ni vacancies (Ni^{+3}) and/or substitution of excess oxygen by nitrogen. This was confirmed by analyzing the XPS spectra of the undoped NiO –P0 and the doped NiO:N P2 films. Fig. 5 depicts the Ni 2p core-level high resolution XPS spectra. The Ni 2p spectra contained two peaks attributed to Ni^{2+} (853.8 eV and 872.2 eV), one peak at 856.0 eV attributed to Ni^{3+} and the other peaks are the satellite-type peaks of Ni $2p_{1/2}$ and Ni $2p_{3/2}$. It should be mentioned that there is a slight shift to lower binding energies of Ni 2p in NiO:N than those in undoped NiO, which is associated with changes in Ni chemical potentials induced upon N-doping with possible extra charges in the Ni side [51,52]. The density of Ni^{+3} ions is generally considered to contribute and have strong dependence on the density of defects in Ni-O

structure [36] as well as being responsible for the coloring of NiO films [40]. As seen in Fig. 5, the intensity as well as the area of Ni^{+3} in XPS spectra of NiO:N are reduced when compared to the undoped NiO. This confirms that the structure of NiO is becoming less defective, and should be more transparent, upon doping with nitrogen.

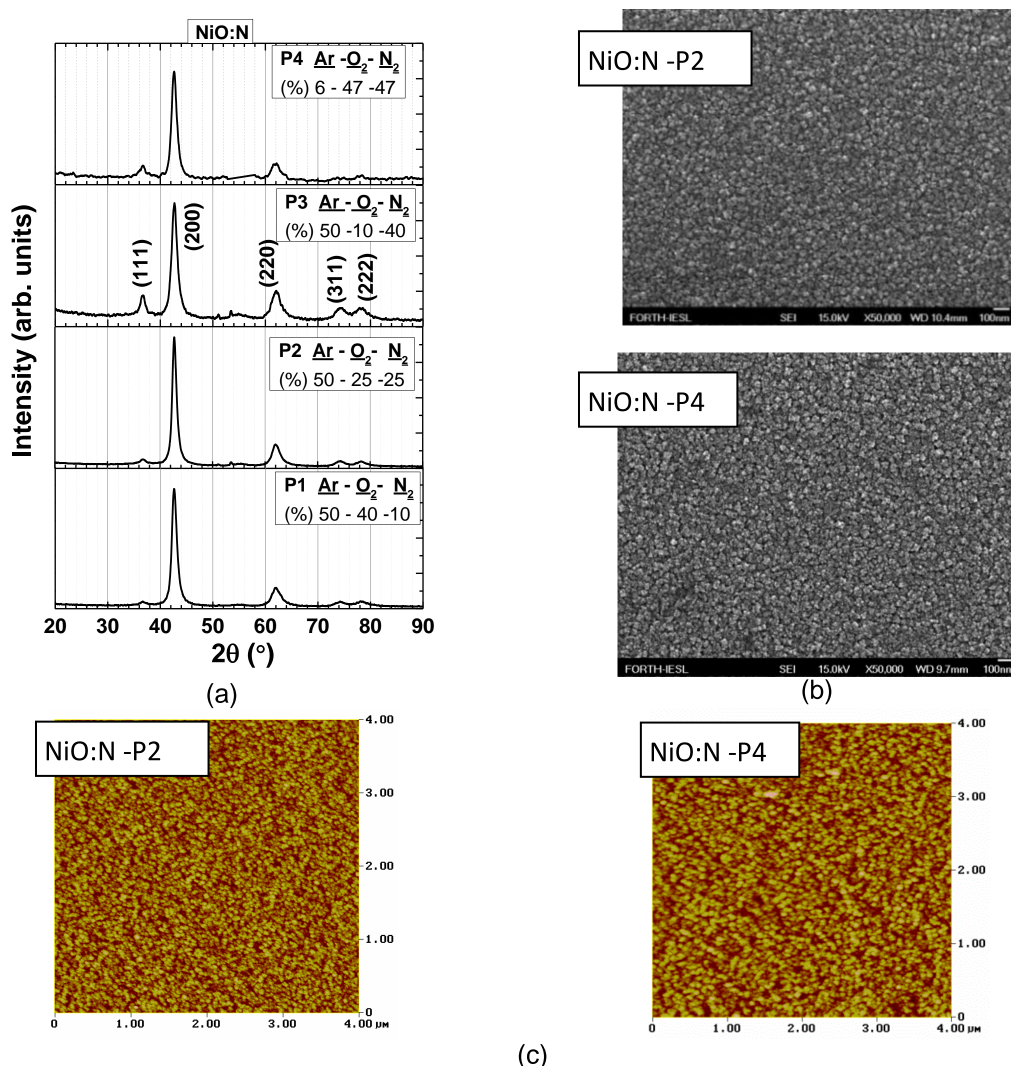

Fig. 4. (a) XRD patterns of N-doped NiO films made in 50% Ar gas in plasma and varying %(O_2-N_2) gases and (b) and (c) SEM and AFM images, respectively, of N-doped NiO films in Ar-rich plasma (50% Ar, film P2) and Ar-deficient plasma (6% Ar, film P4). All films were deposited on Si substrates

The optical properties of NiO:N followed the structural improvements concerning defects and strain when compared to undoped NiO as mentioned above and the films were more transparent. The transmittance, absorption coefficient and the deduced direct energy gap, of nitrogen-doped NiO P1-P4 films are plotted in Fig. 6a and 6b, respectively. The highest transmittance was observed for films deposited having equal O_2 and N_2 flow rates regardless of the amount of Ar in plasma (films P2 and P4 having 50% and 6% Ar gas in plasma, respectively). These films (P2 and P4) had visible transmittance of 45-65% whereas for all other films the optical transmittance was 30-40%. The reflectance of NiO:N films, not shown here, was smaller than the reflectance of the undoped NiO films (less than 20%) throughout the UV-Vis-NIR spectrum range (250-2500 nm). These results were reproducible and independent of thickness, at least for the range of thicknesses examined in this work. The increase in transmittance of N-doped NiO films when compared to the undoped NiO films

could be related to the decrease in Ni vacancies and subsequently fewer Ni^{+3} ions. Although the majority of NiO dopants until now have been cations, such as Li^{+}, Zn^{2+} and Al^{3+}, it is generally agreed that a disordered structure, Ni vacancies and the presence of Ni^{+3} ions have been associated with the low transmittance of NiO. It is anticipated that nitrogen fills Ni vacancies and/or replacing oxygen partially improving NiO stoichiometry, which is in accordance with the observed reduction of at.% of the O/Ni ratio upon introducing nitrogen in the Ni-O structure. The less disordered structure and the decrease in the tensile strain of NiO upon nitrogen doping resulted in more transparent films with a larger energy gap. These observations are not in accordance with theoretical predictions [22] and published experimental work [36-40] for nitrogen-doped NiO, which are presented in Table 1. This is attributed to the quality and stoichiometry of the undoped NiO fabricated by sputtering in this work, such as the preferential growth of crystallites in the [200] direction instead the [111] generally observed and the high ratio of at.% O/Ni~1.72. Loss of transparency and reduction of the energy band gap of NiO upon doping with nitrogen has been reported for films grown preferentially in the [111] direction [38,39], having poor crystallinity [39] or being amorphous [37] or having ratio of at.% O/Ni=1.14 [36].

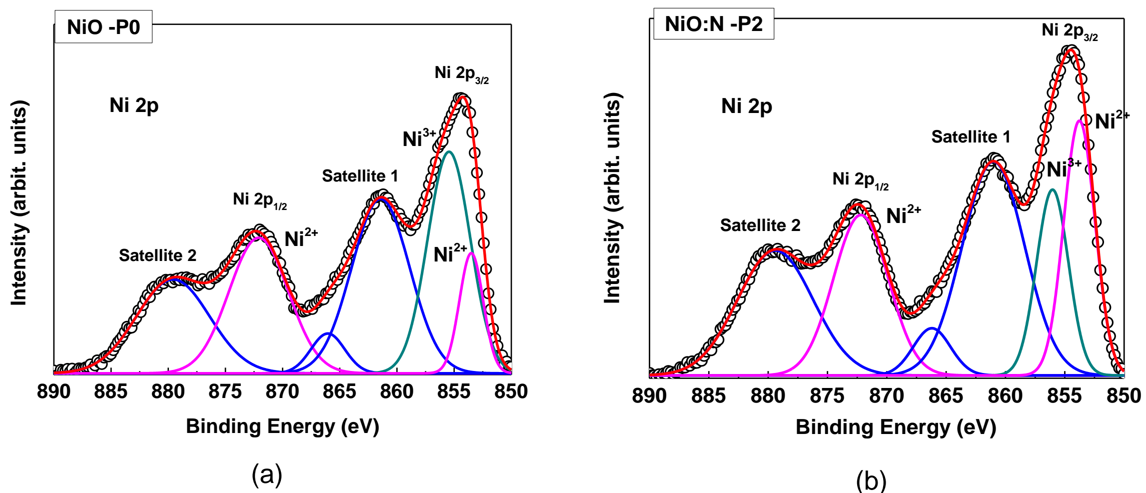

Fig. 5. High resolution Ni 2p core level spectra of (a) undoped NiO –P0 film and (b) nitrogen-doped NiO –P2 film. Open cycles: experimental points, red line: superposition of the de-convoluted peaks (blue, green and pink lines)

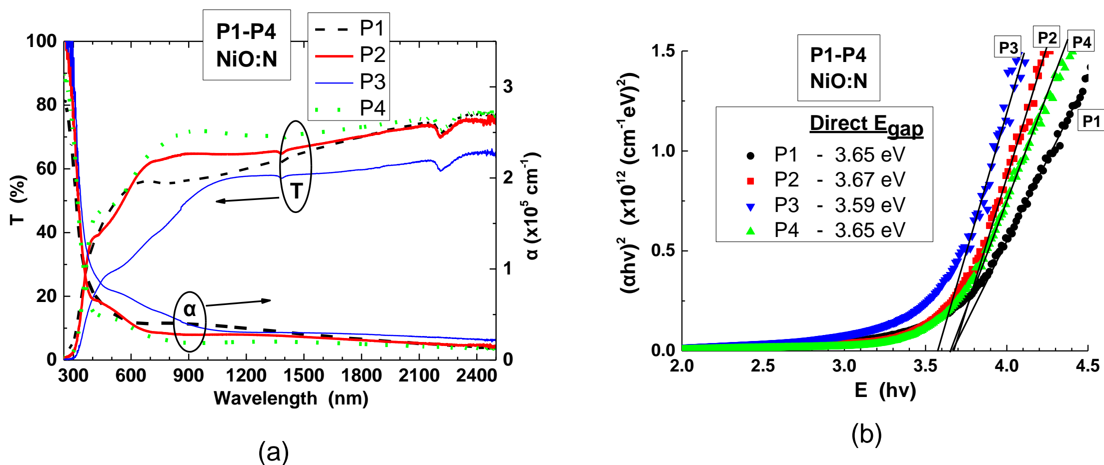

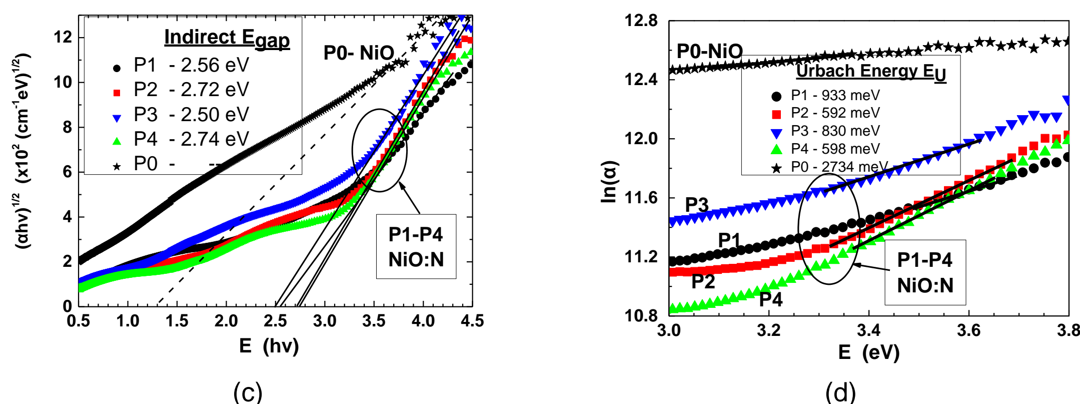

Fig. 6. Optical properties of N-doped NiO films P1-P4 fabricated under different plasma conditions: (a) UV-Vis-NIR transmittance & absorption coefficient curves, (b) (c) and (d) direct band gap, indirect band gap and Urbach tail states energy width determinations, respectively

NiO is considered a direct band gap semiconductor associated with transitions from the top of the valence band to the bottom of the conduction band. The direct band gap is generally determined from spectrophotometric measurements such as UV-Vis-NIR transmittance and reflectance by applying Equation (2) and the Tauc plot of $((\alpha h\nu)^n$-vs-hv) for n=2. In this way, the direct band gap of NiO has been reported ranging from 3.6 to 4 eV. However, there have been reports in which the optical band gap of NiO has been determined to be 3.45 eV [53] or 2.75-2.83 eV [30] by applying the above Tauc plot for n=1/2, which is used for determining the indirect band gap of a semiconductor or having both direct (3.6 eV) and indirect (3.2 eV) band gaps [34]. For the N-doped NiO films of this work, the Tauc plots for both direct and indirect determination of energy band gaps were applied and the results are seen in Fig. 6b and 6c, respectively. The extracted optical band gaps are tabulated in Table 2. For comparison reasons the Tauc plot for the indirect band gap determination of the reference undoped NiO film is also included, although it cannot be defined in a straightforward manner as for the NiO:N films. It can be seen that the increase in visible transmittance upon N-doping is associated with an increase in the direct band gap of NiO from 3.48 eV to 3.64 eV. This observation, as in the case of the increase in the visible transmittance with doping, which was mentioned above, is anticipated to be related to the observation that the undoped NiO of this work was highly disordered. Such a disordered structure is expected to distort the edges of the parabolic bands and the states in the band gap [54,55]. Nitrogen seems to fill nickel vacancies and, because the films become less O-rich upon doping, as mentioned previously, the defects are reduced giving rise to an increase in the energy band gap. By applying the Tauc plot for indirect band gap determination, Fig. 6c, it was revealed that there was clear indication of an indirect band gap for the N-doped NiO films ranging from 2.65 to 2.87 eV depending on the amount of nitrogen in plasma during deposition or equivalently on the amount of nitrogen in the films' structure. On the other hand, no clear indications of the existence of an indirect band gap for the undoped NiO film P0 were seen in Fig. 6c. Furthermore, the values of absorption coefficient seen in Fig. 6a are $\alpha > 10^5$ cm^{-1} for very short wavelengths ($\lambda < 400$ nm), suggesting absorption of photons and transitions between the extended states of both valence and conduction bands (direct allowed transitions) [55]. For longer wavelengths ($\lambda > 400$ nm), however, the absorption coefficient has values $\alpha < 10^5$ cm^{-1}, which implies transitions obeying exponential behavior with photon energy.

It is generally agreed that structural distortions in correlated materials like NiO especially due to doping can significantly affect the electronic structure and defect levels [44]. The non-stoichiometric and disordered NiO, and the NiO:N films of this work, were investigated for the states and their width near the edge of the band gap, namely the Urbach tail states width, the Urbach energy. These shallow states near the edge of valence and/or conduction bands are localized and have been reported for amorphous, polycrystalline oxide and non-oxide materials, such as TiO_2 [56,57], ZnO [58,59], Co_3O_4 [59], Zn-P-V-Mo-O [60], AlN [61], CdSSe [62], metal-organic frameworks (MOFs) [63],

perovskites [64,65] and NiO [27,59,66,67]. These states can extend hundreds of meV above the maximum of valence band edge, and are proportional to structural distortion and vary inversely to the band gap energy. The Urbach tails width can be calculated through the absorption coefficient of the material, α, and the relation [54]: $\alpha = C\exp(E/E_U)$, where E is the photon energy, C is a constant and E_U is the Urbach energy. By plotting ln(α)-vs-E a straight line is obtained, whose inverse slope can give an estimation of the Urbach tail. Fig. 6d shows the lnα-vs-E plots of NiO and NiO:N films (P0-P4), through which the Urbach tail width was determined, as listed in Table 2. It can be seen that for the undoped NiO, being defective and disordered, the gap states extended almost 2.7 eV deep in the band gap. It is anticipated that by introducing nitrogen in NiO, most of these defects in the band gap were compensated leaving states extending up to around 600 meV above the valence band edge. The band gap energies are seen to be inversely proportional to Urbach's tail widths. The NiO:N films P2 and P4 deposited in plasma having equal flow rates for O_2 and N_2 (25:25 and 47:47, respectively), have the narrowest width of Urbach tail states (592 and 598 meV). Based on these experimental results, the energy band gap diagram of the undoped NiO –P0 film and the nitrogen doped NiO –P4 film fabricated by sputtering in Ar-rich and Ar-deficient plasma is proposed in Fig. 7. Urbach tail states have been observed for doped and undoped NiO. Sr-doped NiO has been reported [66] to exhibit increasing width of Urbach states with Sr doping, from 558 meV for the undoped NiO to 892 meV for NiO:Sr. Dependence of Urbach tail width on NiO thickness has been reported, ranging from 600 meV to 1.7 eV for 420 nm and 700 nm thick NiO, respectively, which was reduced to 500 meV upon annealing [27]. It is not known whether the indirect band gap observed for the NiO:N films in this investigation is related to the Urbach tails but it is noticeable that for these films the difference between the values of direct E_{gap} and Urbach energy E_U for each film is almost equal to that of indirect E_{gap}. More experiments are needed to verify the relation between Urbach tails, band gap states and photon- and/or phonon-assisted transitions for nitrogen-containing NiO films [68].

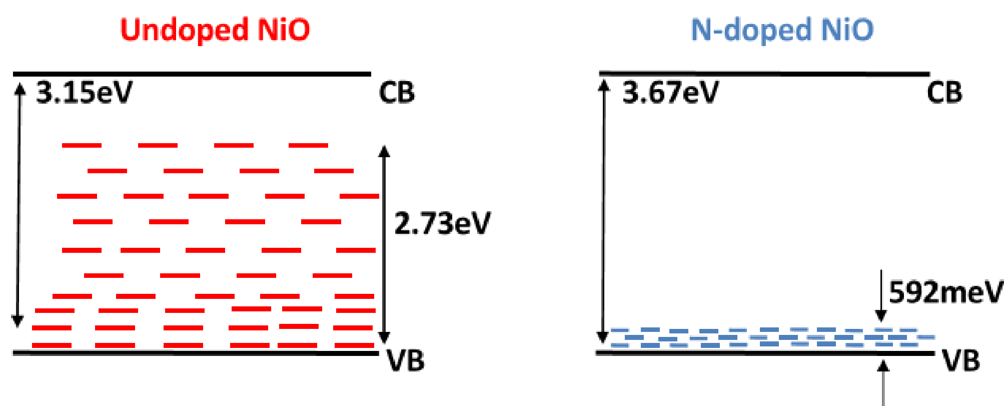

Fig. 7. Typical representation of the energy band gap diagram for the oxygen-rich undoped NiO –P0 film and the nitrogen-doped NiO –P4 film fabricated by sputtering in this study

The resistance of these films was high enough to allow any reliable Hall measurements to be performed. The defective and disordered undoped NiO had resistance, measured between the opposite contact pads of Hall pattern, of a few tens of kΩ. Upon doping with nitrogen, as shown above, the film became less defective and more stoichiometric, leading to an increase in resistance to a few hundreds of kΩ. This observation supports the conclusion that the increase in the energy band gap of NiO:N in this investigation is not associated with an increase in holes' concentration due to the Moss-Burstein effect, according to which increase in carrier concentration results in an increase in energy band gap [69]. Deterioration of the electrical properties and improvement of optical properties have been reported for NiO:Cu films when co-doped with nitrogen [43]. It is the first time to our knowledge in which the introduction of nitrogen in NiO films is reported to improve its optical transmittance, paving the way for applying NiO:N films in transparent and flexible optoelectronic applications such as perovskite solar cells and UV detectors.

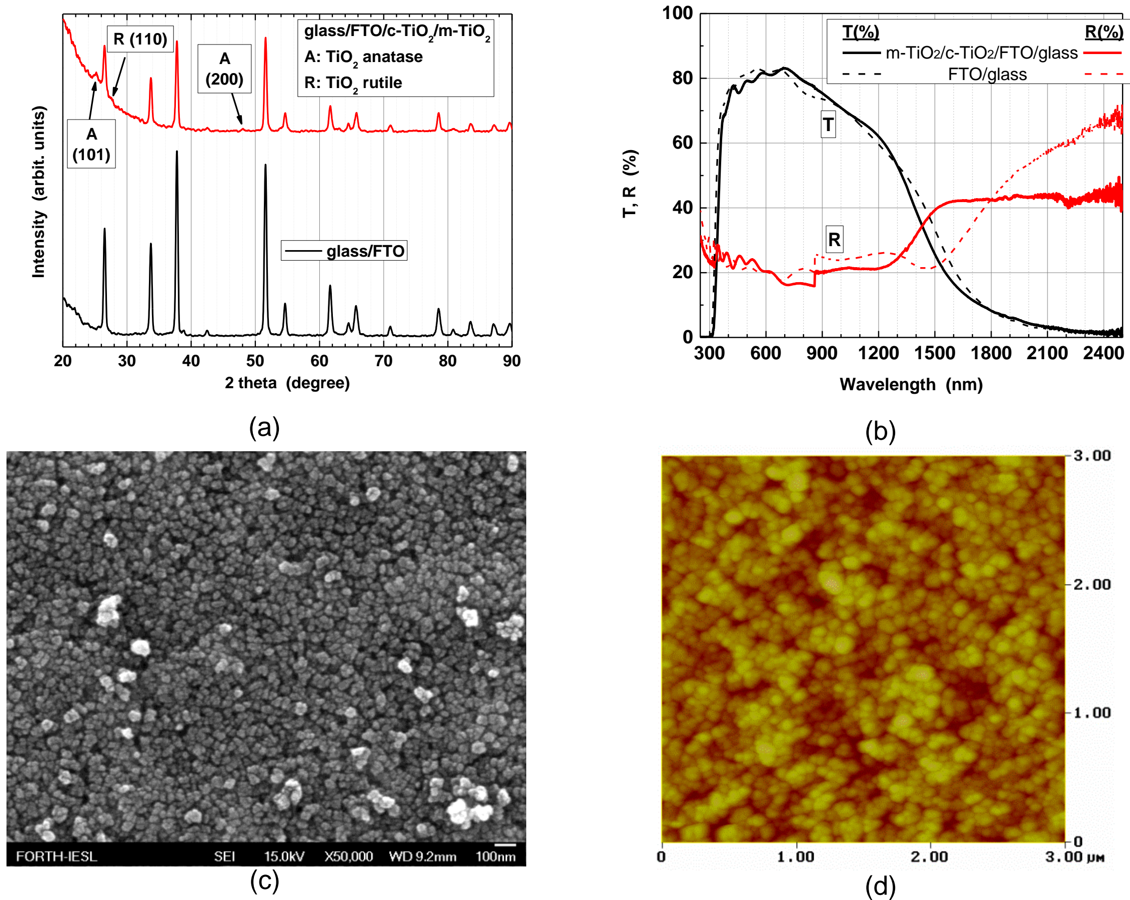

Fig. 8. (a) XRD patterns and (b) UV-Vis-NIR transmittance and reflectance curves of m-TiO$_2$/c-TiO$_2$/FTO/glass and FTO/glass and (c) SEM surface image of m-TiO$_2$/c-TiO$_2$/FTO/glass

3.1.2 Properties of TiO$_2$ thin film

The n-type TiO$_2$ thin films used for forming the heterojunction with the transparent NiO:N film was a two-layers TiO$_2$ thin film, namely a mesoporous TiO$_2$ layer (m-TiO$_2$) on top of a compact TiO$_2$ layer (c-TiO$_2$). Both layers were formed by spin-coating on FTO/glass substrate, as described in the Materials and Methods section. The XRD pattern, the surface morphology and the transmittance and reflectance of the m-TiO$_2$/c-TiO$_2$/FTO/glass configuration are seen in Fig. 8. As seen in Fig. 8a, the XRD pattern of TiO$_2$ layers was dominated by the peaks arising from the underneath FTO layer, whose crystallite size, as deduced for the peak at 37.8^o using the Scherrer formula, was 21.7 nm. The diffraction peaks originating from TiO$_2$ had a very small intensity and were ascribed to the anatase phase (JCPDS card number 01-071-1167) and the rutile phase (JCPDS card number 01-076-0319). The transmittance and reflectance of m-TiO$_2$/c-TiO$_2$/FTO/glass and those of FTO/glass are seen in Fig. 8b. TiO$_2$ did not affect the optical properties of the FTO/glass. The visible transmittance and reflectance of the m-TiO$_2$/c-TiO$_2$/FTO /glass were 75-85% and 15-25%, respectively. The surface of the m-TiO$_2$ was rough (Fig. 8c) with RMS roughness of 20 nm (Fig. 8d).

3.2 Characterization of the p-NiO:N/n-TiO$_2$ Diode

The m-TiO$_2$/c-TiO$_2$/FTO /glass was used as a substrate on which the N-doped NiO –P2 film was sputtered in plasma containing flow rates ratio (%) Ar:O$_2$:N$_2$=50:25:25. As shown previously (Table 2), film P2 was chosen to form the heterojunction because it had the optimum structural and optical properties, such as less lattice strain, higher visible transmittance, wider band gap and the narrowest

Urbach width, compared to all other films examined. The width of Urbach states was the second most-important criterion following transmittance because these states can appear as states at the NiO:N-TiO_2 interface, affecting the rectifying output characteristics of the diode [70]. The transmittance and reflectance of the fabricated NiO:N/TiO_2 diode is presented in Fig. 9a, along with those of TiO_2 for comparison reasons. It is seen that the visible transmittance of m-TiO_2/c-TiO_2/FTO/glass (75-85%) drops to the value of 40-55% after depositing the NiO:N –P2 film on the surface of m-TiO_2/c-TiO_2/FTO/glass. Similar transmittance values have been reported for sputtered NiO/TiO_2 [71] or NiO/ZnO [72] diodes. The visible reflectance was around 20%, whereas the near-IR reflectance was around 75% and the respective transmittance was less than 10%. The high value of near-IR reflectance of this configuration of layers indicates potential use in chromogenic applications [73,74]. In addition, the strong cut-off of ultraviolet (UV) wavelength photons indicates strong absorption of UV light for the all-oxide layers, thus making the diode a strong candidate for transparent optoelectronic applications. It is worth mentioning that XRD measurements were performed on the diode but the diffraction peaks were very noisy and could not be identified as arising from any of the layers of the diode due to the very rough surface of the spin-coated TiO_2 layers seen in Fig. 8c,d. One of the motivations of this investigation was the fabrication of all-oxide heterodiodes with enhanced visible transparency. For this reason, the as-prepared NiO:N/TiO_2 heterostructure was annealed at higher temperatures. The transmittance of the NiO:N/TiO_2 just after fabrication and after thermal treatment at 500 ^{o}C (TT3) is plotted in Fig. 9b. The visible transmittance of the as-prepared NiO:N/m-TiO_2/c-TiO_2/FTO/glass heterostructure is increased by around 35% after post-deposition annealing up to 500 ^{o}C (TT3), from the value of around 50% to around 65%. As described in the Materials and Methods section, the TiO_2 layers, the mesoporous m-TiO_2 and the compact c-TiO_2, had already undergone thermal treatments at 500 ^{o}C during fabrication of these layers. Thus, the improvement of visible transmittance of NiO:N/m-TiO_2/c-TiO_2/FTO/glass diode upon thermal treatment are expected to be mainly due to improvement of the optical characteristics of the NiO:N layer with annealing. This was evidenced after depositing a NiO:N –P2 film on glass substrate, annealing it up to 500 ^{o}C (TT3) and monitoring its UV-Vis-NIR transmittance. The transmittance of a NiO:N/glass film after thermal treatment (TT3) is plotted in Fig. 9b, along with the transmittance curves of the NiO:N/m-TiO_2/c-TiO_2/FTO/glass heterostructure. It is apparent that the relatively low visible transmittance of the as-prepared NiO:N –P2 film of 40-60% (seen in Fig. 6a) increased to 65-87% upon thermal treatment (Fig. 9b) due to improvement of structure crystallinity. From the transmittance curves of NiO:N film just after deposition (Fig. 6a,b) and after thermal treatment TT3 (Fig. 9b) it is extracted that the direct and indirect energy gaps of NiO:N –P2 film are increased from 3.67 eV and 2.72 eV (Table 2) to 3.75 eV and 3.38 eV, respectively, whereas the Urbach tail width was decreased from 592 meV (Table 2) to 217 meV. Similar energy band gap values have been reported for NiO:N films made by the sol-gel technique at 120°C followed by post-formation thermal treatment at 450°C for 1 hour [37]. The transparency achieved for the NiO:N/m-TiO_2/c-TiO_2/FTO/glass after thermal treatment is also seen in the inset of Fig. b, where a photograph of the fabricated NiO:N/TiO_2 heterostructure with Au dot metal contacts is shown.

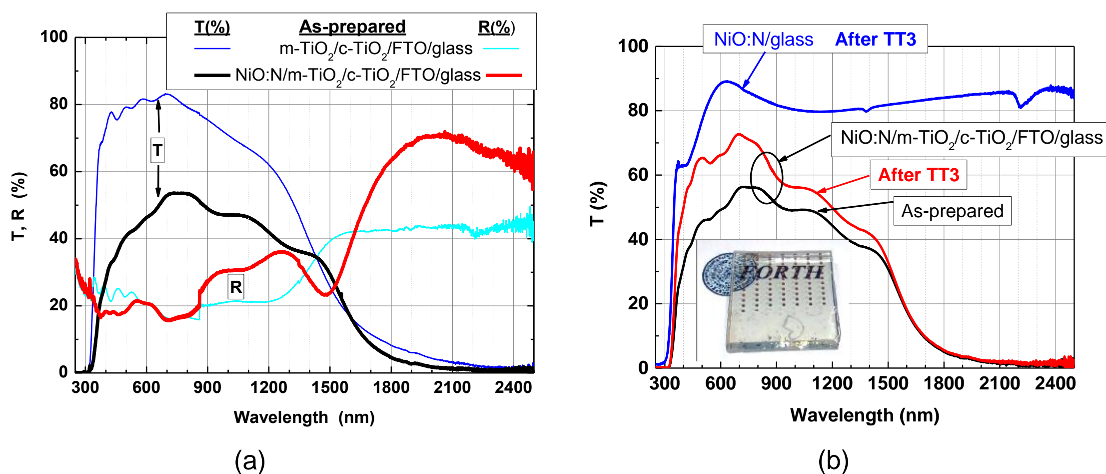

(a) (b)

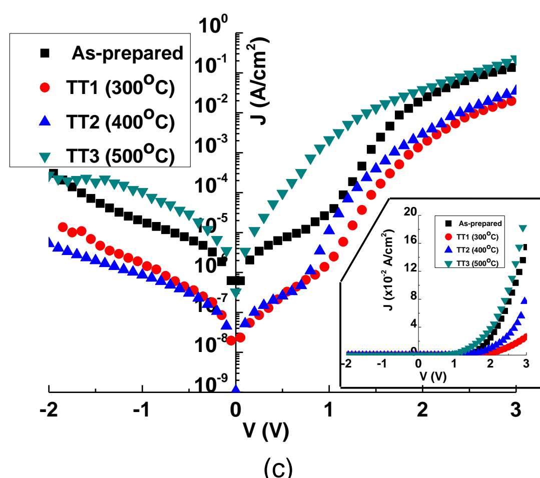

(c)

Fig. 9. (a) UV-Vis-NIR transmittance and reflectance curves of as-prepared NiO:N/m-TiO_2/c-TiO_2/FTO/glass diode and m-TiO_2/c-TiO_2/FTO/glass configurations. (b) Transmittance curves of NiO:N/m-TiO_2/c-TiO_2/FTO/glass diode after fabrication and after annealing (TT3=500°C). The inset shows a typical NiO:N/m-TiO_2/c-TiO_2/FTO/glass diode after TT3 with Au dots. (c) Dark J-V curves (semi-log and linear scales) of NiO:N/m-TiO_2/c-TiO_2/FTO diode just after fabrication and after successive thermal treatments (TT) up to 500 °C

The linear and semi-log dark current density-voltage (J-V) characteristics of the Au/NiO:N/m-TiO_2/c-TiO_2/FTO/glass diode are seen in Fig. 9c just after fabrication and after successive thermal treatments up to 500°C. Rectification behavior can be seen for the as-prepared diode, whereas heat treatment improved its characteristics. The rectification ratio (forward current density to reverse current density, J_f/J_r) at ±1.5 V was J_f/J_r=29 before any heat treatment, it was slightly reduced to J_f/J_r=23 after TT1 and increased to J_f/J_r=200 and J_f/J_r=710 after TT2 and TT3, respectively. It is also observable at the semi-log J-V curves of Fig. 9c that the shoulder seen for V_f < 1V for the diode after fabrication and after thermal treatments at TT1 and TT2 (i.e., less than 500°C) almost disappears after annealing at 500°C (TT3). These observations concerning the shape of the diode's J-V curves with thermal treatment are reflected in the diode's parameters, which are calculated below. The parameters of the diode, such as saturation current density (J_S), barrier height (Φ_b), ideality factor (n) and series resistance (R_S), were obtained following thermionic emission theory from the I-V curve [75] and by applying Cheung's method [76]. Assuming thermionic emission over the barrier of a diode and for V>3kT/q, the standard diode equation is [75]:

$$I = I_s \exp\left(\frac{qV}{nkT}\right) \quad (3)$$

where T is the temperature in Kelvin (K), *q* is the electron charge and k is the Boltzmann constant. The above equation can be written as $\ln(I)=\ln(I_S)+(q/nkT)V$, from which by plotting ln(I)-vs-V, n and I_S can be deduced from the slope and the intercept of line with the ln(I) axis, respectively. The barrier height, Φ_b was determined from:

$$I_S=AA^*T^2\exp(-q\Phi_b/kT)$$

where A is the diode area and A^* is the Richardson constant (120 A/cm^2K^2 [30,76]). The series resistance R_S of the diode was extracted from the I-V curve for V>2V [77], independently from Equation (3) and thermionic emission theory.

For extracting the diode characteristics using Cheung's approach [76], which takes into account the effect of R_S, Equation (1) is written as:

$$I = I_s \exp\left(\frac{q(V-IR_S)}{nkT}\right) \tag{4}$$

From Equation (4), the quantity $\frac{dV}{d(\ln I)} = \frac{nkT}{q} + I \cdot R_s$ can be derived from which by plotting $\frac{dV}{d(\ln I)}$-vs-I, the slope gives R_S and the intercept gives n. By defining $H=V-\frac{nkT}{q}\ln\left(\frac{I}{AA^*T^2}\right)$, the equation $H = n\Phi_b+R_SI$ can be derived, from which the graph of H-vs-I can give R_S and Φ_b from the slope and the intercept, respectively. The results for the characteristics of the NiO:N/m-TiO_2/c-TiO_2/FTO diode just after fabrication and after thermal treatments, obtained from the I-V curves of Fig. 9c by applying Equations (3) and (4) for thermionic emission theory and Cheung's method, respectively, are tabulated in Table 3.

Table 3. NiO:N/m-TiO_2/c-TiO_2/FTO diode characteristics before and after thermal treatments (TT): saturation current density (J_S), barrier height (Φ_b), ideality factor (n) and series resistance (R_S), after applying I-V and Cheung's methods. TT1 = 300°C, TT2 = 400°C and TT3 = 500°C

Treatment	I-V method				Cheung's method			
	J_s (A/cm^2)	R_s (Ohm)	n	φ_b (eV)	J_s (A/cm^2)	R_s (Ohm)	n	φ_b (eV)
As-prepared	5.0×10^{-9}	8.5×10^{2}	4.6	0.91	1.5×10^{-6}	7.2×10^{2}	7.6	0.77
TT1	2.8×10^{-10}	1.4×10^{4}	4.4	0.99	1.9×10^{-7}	3.0×10^{3}	8.4	0.82
TT2	3.3×10^{-10}	9.8×10^{3}	3.8	0.98	1.4×10^{-6}	2.6×10^{3}	9.9	0.77
TT3	3.3×10^{-6}	1.8×10^{3}	5.8	0.75	1.6×10^{-12}	3.5×10^{2}	3.5	1.12

The diode formed between NiO:N and m-TiO_2/c-TiO_2 showed reasonable, good parameters and both methods used for analyzing the characteristics of the diode revealed that annealing improved the diode's output characteristics. The saturation current density, J_S and the barrier height, which is inversely proportional to J_S, have similar values to those reported in the literature for NiO-containing diodes [27,30,72]. The ideality factor, n, is a parameter indicating whether the diode obeys the thermionic emission model in which n should be $1 < n < 2$. Because the diode has $n > 2$ implies that the transport mechanism is not dominated by thermionic emission but through recombination at defects/states at the interface, tunneling through the interfacial layer or space charge current transport [30]. The diodes' characteristics are known to generally improve with thermal treatment [76,78-80] and this was the case for the NiO:N/TiO_2 heterodiodes annealed up to 400°C (TT2) and seen in Table 3. Annealing, however, at higher temperature, TT3=500°C, the analysis of diode's parameters using the I-V and Cheung methods gave contradicting results. The diode parameters, which are improved with annealing, are anticipated to be partially related to the improved crystallinity of NiO:N, reduction of structural defects and Urbach tails width, as mentioned above, and consequently reduced NiO:N/TiO_2 interface states. It should be recalled that the NiO:N/TiO_2 diode is a hybrid diode because NiO:N was sputter-deposited on unheated substrates whereas the spin-coated formed TiO_2 layers had undergone annealing at 500°C. The diode's series resistance, R_S, is less than 1 kΩ just after fabrication but it is increased after the first annealing treatments (TT1 and TT2), probably due to the increased resistance of NiO:N with annealing, and decreased again after TT3. More experiments are needed to identify the origin of the diode's behavior with thermal treatment. Finally, it is the first time that Cheung's method has been applied for analyzing a NiO/TiO_2 diode and the different results observed between the two methods, used for extracting the diode's parameters as seen in Table 3, have been also observed for NiO/ITO [31] and for epitaxially grown AlGaAs diodes [79]. The differences might be attributed to the fact that Cheung's model takes into account the series resistance of the diode (Equation (4)) and is applied to the whole range of forward voltages, whereas the I-V method is applied for voltages where the linear part of the I-V curve starts, i.e., $V > 3$ kT/q = 0.78 V [31]. Improvement of diode characteristics can be accomplished by further optimizing the fabrication procedure, such as TiO_2 surface treatment prior to the NiO deposition [29]. More experiments are needed for evaluating the diode's behavior, if this type of diode is to be used for flexible and/or transparent optoelectronic applications, such as tandem perovskite solar cells and UV photovoltaics.

4. CONCLUSION

A transparent hybrid heterodiode was fabricated by employing sputtered NiO:N and spin-coated TiO_2 as p-type and n-type layers respectively. The reference undoped NiO was fabricated by sputtering a Ni target on room temperature substrates in plasma containing 50% Ar and 50% O_2. The nitrogen-containing films (less than 1.5 at.% of nitrogen) were fabricated in 50% Ar and 50% (O_2 +N_2) gases by gradually substituting O_2 with nitrogen in plasma (0%-40% N_2). Upon nitrogen doping, the O-rich undoped NiO film became less disordered and more transparent. The direct and possible indirect band gaps of NiO:N, in addition to the subgap states, the Urbach tail states, were correlated with the amount of nitrogen in plasma during deposition. The optimum NiO:N film, fabricated in plasma containing equal amounts of O_2 and N_2 gases (50%Ar/25%O_2/25%N_2) had the highest transmittance (49.1%), widest band gap (3.67 eV direct and 2.72 eV indirect gaps) and the narrowest Urbach width (592 meV) compared to the other films of this investigation. The optimum NiO:N film was used to form a heterojunction on spin-coated mesoporous TiO_2 on top of compact-TiO_2/FTO/glass. The NiO:N/m-TiO_2/c-TiO_2/FTO/glass heterostructure showed rectification properties, which were analyzed by employing the I-V and Cheung' methods. Most of the output characteristics of the diode, including transparency, were improved upon thermal treatment and the changes were associated with improvements in NiO:N properties, such as transparency and less Urbach tail states and the NiO:N/m-TiO_2 interface with annealing. The nitrogen-doped NiO fabricated in this work can be used for realizing transparent and flexible devices for wearable and optoelectronic applications.

FUNDING

This work was partially supported by the projects "Materials and Processes for Energy and Environment Applications-AENAO" (MIS 5002556) and "NANOTANDEM" (MIS 5029191) co-financed by Greece and EU (European Regional Development Fund).

ACKNOWLEDGEMENTS

We are grateful to Dr. E. Spanakis of Materials Science & Technology Dept., of Crete University for performing the XPS experiments.

COMPETING INTERESTS

Authors have declared that no competing interests exist.

REFERENCES

1. Osorio-Guillén J, Lany S, Zunger A. Non-stoichiometry and hole doping in NiO, AIP Conference Proceedings. 2010;1199:128-129.
DOI: 10.1063/1.3295330.
2. Karsthof R, Grundmann M, Anton AM, Kremer F. Polaronic inter-acceptor hopping transport in intrinsically doped nickel oxide, Phys. Rev. B. 2019;99:235201.
DOI: 10.1103/PhysRevB.99.235201(13pp)
3. Zou ZG, Ye JH, Sayama K, Arakawa H. Direct splitting of water under visible light irradiation with an oxide semiconductor photocatalyst, Nature. 2001;414:625-627.
DOI: 10.1038/414625a
4. Charisiadis A, Glymenaki E, Planchat A, Margiola S, Lavergne-Bril AC, Nikoloudakis E, Nikolaou V, Charalambidis G, Coutsolelos AG, Odobel F. Photoelectrochemical properties of dyads composed of porphyrin/ruthenium catalyst grafted on metal oxide semiconductors, Dyes and Pigments. 2021;185:108908(12pp).
DOI: 10.1016/j.dyepig.2020.108908.
5. Rosado PC, Meyrelles R, Macatrão AM, Justino MC, Gomes AG, Montemor MF, et al. Immobilization of His-tagged proteins on NiO foams for recyclable enzymatic reactors, Appl. Sur. Sci. 2021;537:147848(8pp).
DOI: 10.1016/j.apsusc.2020.147848

6. Yang S, Lei G, Xu H, Lan Z, Wang Z, Gu H. Metal Oxide Based Heterojunctions for Gas Sensors: A Review, Nanomaterials. 2021;11:1026 (26pp).
DOI: 10.3390/nano11041026
7. Gagaoudakis E, Michail G, Kampylafka V, Tsagaraki K, Aperathitis E, Moschovis K, et al. Room Temperature p-Type NiO Nanostructure Thin Film Sensor for Hydrogen and Methane Detection, Sensor Letters. 2017;15:663- 667.
DOI: 10.1166/sl.2017.3864
8. Mokoena TP, Swart HC, Motaung DE. A review on recent progress of p-type nickel oxide based gas sensors: Future perspectives, J. Alloys and Compounds. 2019;805:267-294.
DOI: 10.1016/j.jallcom.2019.06.329
9. Zhang J, Yu A. Nanostructured transition metal oxides as advanced anodes for lithium-ion batteries, Sci. Bull. 2015;60:823-838.
DOI: 10.1007/s11434-015-0771-6
10. Wang Z, Wang X, Cong S, Geng F, Zhao Z. Fusing electrochromic technology with other advanced technologies: A new roadmap for future development, Mat. Sci. & Engineering R. 2020;140:100524(26pp).
DOI: 10.1016/j.mser.2019.100524
11. Pansri S, Supruangnet S, Nakajima R, Rattanasuporn H, Noothongkaew SS. Band offset determination of p-NiO/n-TiO_2 heterojunctions for applications in high-performance UV photodetectors, J. Mater. Sci. 2020;55:4332–4344.
DOI: 10.1007/s10853-019-04305-x
12. Karsthof R, von Wenckstern H, Zúniga-Pérez J, Deparis C, Grundmann M. Nickel Oxide–Based Heterostructures with Large Band Offsets, Phys. Status Solidi B. 2020;257:1900639(11pp).
DOI: 10.1002/pssb.201900639
13. Grundmann M, Klüpfel F, Karsthof R, Schlupp P, Schein FL, Splith D, Yang C, Bitter S, von Wenckstern H. Oxide bipolar electronics: materials, devices and circuits, J. Phys. D: Appl. Phys. 2016;49:213001(25pp).
DOI: 10.1088/0022- 3727/49/21/213001
14. Nguyen TT, Patel M, Kim S, Mir RA, Yi J, Dao VA, Kim J. Transparent photovoltaic cells and self-powered photodetectors by TiO_2/NiO heterojunction, J. Power Sources. 2021;481:228865,
DOI: 10.1016/j.jpowsour.2020.228865
15. Tirado J, Vásquez-Montoya M, Roldán-Carmona C, Ralaiarisoa M, Koch N, Nazeeruddin MK, Jaramillo F. Air-Stable n–i–p Planar Perovskite Solar Cells Using Nickel Oxide Nanocrystals as Sole Hole-Transporting Material, ACS Appl. Energy Mater. 2019;2:4890-4899.
DOI: 10.1021/acsaem.9b00603
16. Elseman AM, Sajid SE, Shalan A, Mohamed SA, Rashad MM. Recent progress concerning inorganic hole transport layers for efficient perovskite solar cells, Appl. Phys A. 2019;125:476(12pp).
DOI: 10.1007/s00339-019-2766-7
17. Chai W, Zhu W, Chen D, Chen D, Xi H, Chang J, Zhang J, Zhang C, Hao Y. Combustion-processed NiO/ALD TiO_2 bilayer as a novel low-temperature electron transporting material for efficient all-inorganic $CsPbIBr_2$ solar cell, Solar Energy. 2020;203:10–18.
DOI: 10.1016/j.solener.2020.04.024.
18. Predanocy M, Hotovy I, Caplovicová M. Structural optical and electrical properties of sputtered NiO thin films for gas detection, Appl. Surf. Sci. 2017;395:208–213.
DOI: 10.1016/j.apsusc.2016.05.028
19. Yang JL, Lai YS, Chen JS. Effect of heat treatment on the properties of non- stoichiometric p-type nickel oxide films deposited by reactive sputtering, Thin Solid Films. 2005;488:242–246.
DOI: 10.1016/j.tsf.2005.04.061
20. Hwang JD, Ho TH. Effects of oxygen content on the structural, optical, and electrical properties of NiO films fabricated by radio-frequency magnetron sputtering, Mat. Sci. Semicond. Processing. 2017;71:396-400.
DOI: 10.1016/j.mssp.2017.09.002
21. Nandy S, Saha B, Mitra MK, Chattopadhyay KK. Effect of oxygen partial pressure on the electrical and optical properties of highly (200) oriented p-type $Ni_{1-x}O$ films by DC sputtering, J. Mater. Sci. 2007;42:5766-5772.
DOI: 10.1007/s10853-006- 1153-x

22. Nolan M, Long R, English NJ, Mooney DA. Hybrid density functional theory description of N- and C-doping of NiO", J. Chem. Phys. 2011;134:224703(8pp).
DOI: 10.1063/1.3596949
23. Zhang L, Staar P, Kozhevnikov A, Wang YP, Trinastic J, Schulthess T. DFT+DMFT calculations of the complex band and tunneling behavior for the transition metal monoxides MnO, FeO, CoO, and NiO, Phys. Rev. B. 2019;100:035104(15pp).
DOI: 10.1103/PhysRevB.100.035104
24. Kim DS, Lee HC. Nickel vacancy behavior in the electrical conductance of non- stoichiometric nickel oxide film, J. Appl. Phys. 2012;112:034504(4pp).
DOI: 10.1063/1.4742993
25. Zhang KHL, Xi K, Blamire MG, Egdell RG. P-type transparent conducting oxides, J. Phys.: Condens. Matter. 2016;28:383002(19pp).
DOI: 10.1088/0953- 8984/28/38/383002
26. Uddin MT, Nicolas Y, Olivier C, Jaegermann W, Rockstroh N, Junge H, Toupance T. Band alignment investigations of heterostructures NiO/TiO_2 nanomaterials used as efficient heterojunction earth-abundant metal oxide photocatalysts for hydrogen production, Phys. Chem. Chem. Phys. 2017;19:19279-19288.
DOI: 10.1039/c7cp01300k
27. Klochko NP, Kopach VR, Tyukhov II, Zhadan DO, Klepikova KS, Khrypunova GS, et al. Metal oxide heterojunction (NiO/ZnO) prepared by low temperature solution growth for UV-photodetector and semi-transparent solar cell, Solar Energy. 2018;164:149–159.
DOI: 10.1016/j.solener.2018.01.054
28. Dey S, Nag S, Santra S, Ray SK, Guha PK. Voltage-controlled NiO/ZnO p–n heterojunction diode: A new approach towards selective VOC sensing, Microsyst. Nanoeng. 2020;6:35(9pp).
DOI: 10.1038/s41378-020-0139-1
29. Xiao Y, Li X, Gong H, Liu W, Wu X, Ding S, Lu H, Ye J. Demonstration of Ni/NiO_x/β-Ga_2O_3 heterojunction diode with F plasma pre-treatment for reducing on-resistance and reverse leakage current, Appl. Sur. Sci. 2022;578:152047.
DOI: 10.1016/j.apsusc.2021.152047
30. Peng WB, Zhou YJ, Xiang GJ, Liu Y, Zhang JH, Zhang JM, et al. Preparation of AlN thin film and the impacts of AlN buffer layer on the carrier transport properties of p-NiO/n-InN heterojunction by magnetron sputtering, Materials Science in Semiconductor Processing. 2022;141:106417.
DOI: 10.1016/j.mssp.2021.106417
31. Wu CC, Yang CF. Effect of annealing temperature on the characteristics of the modified spray deposited Li-doped NiO films and their applications in transparent heterojunction diode, Solar Energy Materials & Solar Cells. 2015;132:492-498.
DOI: 10.1016/j.solmat.2014.09.017
32. Nandy S, Maiti UN, Ghosh CK, Chattopadhyay KK. Enhanced p-type conductivity and band gap narrowing in heavily Al doped NiO thin films deposited by RF magnetron sputtering, J. Phys.: Condens. Matter. 2009;21:115804(7pp).
DOI: 10.1088/0953-8984/21/11/115804
33. Adler D, Feinleib J. Electrical and Optical Properties of Narrow-Band Materials, Phys. Rev. B. 1970;2:3112-3134.
34. Park G, Lee KH, Lee JH, Bang G, Kim J, Park HJ, et al. Improved polaronic transport under a strong Mott–Hubbard interaction in Cu substituted NiO, Inorg. Chem. Front. 2020;7:853-858.
DOI: 10.1039/c9qi01052a
35. Popescu I, Skoufa Z, Heracleous E, Lemonidou A, Marcu IC. A study by electrical conductivity measurements of the semiconductive and redox properties of Nb-doped NiO catalysts in correlation with the oxidative dehydrogenation of ethane, Phys. Chem. Chem. Phys. 2015;17:8138-8147.
DOI: 10.1039/c5cp00392j
36. Keraudy J, Ferrec A, Richard-Plouet M, Hamon J, Goullet A, Jouan PY. Nitrogen doping on NiO by reactive magnetron sputtering: A new pathway to dynamically tune the optical and electrical properties, Appl. Surf. Sci. 2017;409:77-84.
DOI: 10.1016/j.apsusc.2017.02.229

37. Ganesh V, Haritha L, Anisc M, Shkira M, Yahia IS, Singh A, AlFaify S. Structural, morphological, optical and third order nonlinear optical response of spin- coated NiO thin films: An effect of N doping, Solid State Sciences. 2018;86:98-106.
DOI: 10.1016/j.solidstatesciences.2018.10.009
38. Sriram S, Thayumanavan A, Ravichandran K. Influence of nitrogen doping on properties of NiO films, Surf. Engin. 2016;32:207-211.
DOI: 10.1179/1743294414Y.0000000380
39. Zhou P, Li B, Fang Z, Zhou W, Zhang M, Hu W, Chen T, Xiao Z, Yang S. Nitrogen-Doped Nickel Oxide as Hole Transport Layer for High-Efficiency Inverted Planar Perovskite Solar Cells, Sol. RRL. 2019;3:1900164(8pp).
DOI: 10.1002/solr.201900164
40. Tian Y, Gong L, Qi X, Yang Y, Zhao X. Effect of Substrate Temperature on the Optical and Electrical Properties of Nitrogen-Doped NiO Thin Films, Coatings. 2019;9:634(10pp).
DOI: 10.3390/coatings9100634
41. Tangwancharoen S, Thongbai P, Yamwong T, Maensiri S. Dielectric and electrical properties of giant dielectric (Li, Al)-doped NiO ceramics, Mat. Chem. and Phys. 2009;115:585-589.
DOI: 10.1016/j.matchemphys.2009.01.004
42. Dong D, Wang W, Barnabe A, Presmanes L, Rougier A, Dong G, et al. Enhanced electrochromism in short wavelengths for NiO:(Li, Mg) films in full inorganic device ITO/NiO:(Li, Mg)/Ta2O5/WO3/ITO, Electrochimica Acta. 2018;263:277-285.
DOI: 10.1016/j.electacta.2018.01.049
43. Wen CK, Xin YQ, Chen SC, Chuang TH, Chen PJ, Sun H. Comparison of microstructural and optoelectronic properties of NiO:Cu thin films deposited by ion- beam assisted rf sputtering in different gas atmospheres, Thin Solid Films. 2019;677:103-108.
DOI: 10.1016/j.tsf.2019.03.018
44. Wrobel F, Park H, Sohn C, Hsiao HW, Zuo JM, Shin H, Lee HN, Ganesh P, Benali AP, et al. Doped NiO: The mottness of a charge transfer insulator, Phys. Rev. B. 2020;101:195128(15pp).
DOI: 10.1103/PhysRevB.101.195128
45. Raju K, Rajendran S, Hoang TKA, Durgalakshmi D, Qin J, Diaz-Droguett DE, et al. Photosynthesis of H_2 and its storage on the Bandgap Engineered Mesoporous $(Ni^{2+}/Ni^{3+})O@TiO_2$ heterostructure, J. Power Sources. 2020;466:228305.
DOI: 10.1016/j.jpowsour.2020.228305
46. Yu C, Li M, Yang D, Pan K, Yang F, Xu Y, Yuan L, Qu Y, Zhou W. NiO nanoparticles dotted TiO_2 nanosheets assembled nanotubes P-N heterojunctions for efficient interface charge separation and photocatalytic hydrogen evolution" Appl. Sur. Sci. 2021;568:150981.
DOI: 10.1016/j.apsusc.2021.150981
47. Aftab M, Butt MZ, Ali D, Bashir F, Aftab ZH. Impact of copper doping in NiO thin films on their structure, morphology, and antibacterial activity against Escherichia Coli, Ceramics International. 2020;46:5037–5049.
DOI: 10.1016/j.ceramint.2019.10.247
48. Pankove J. Optical Processes in Semiconductors, Dover Publications, NY. 1971;87 (Ch. 4).
49. Jafar MMAG. Comprehensive formulations for the total normal-incidence optical reflectance and transmittance of thin films laid on thick substrates, European International Journal of Science and Technology. 2013;2:214-274.
ISSN: 2304-9693.
Available:www.cekinfo.org.uk/EIJST
50. Himmerlich M, Koufaki M, Ecke G, Mauder Ch, Cimalla V, Schaefer JA, et al. Effect of Annealing on the Properties of Indium−Tin−Oxynitride Films as Ohmic Contacts for GaN-Based Optoelectronic Devices, ACS Appl. Mater. Interfaces. 2009;1:1451-1456.
DOI: 10.1021/am900138f
51. Qian J, Bai X, Xi S, Xiao W, Gao D, Wang J. Bifunctional Electrocatalytic Activity of Nitrogen-Doped NiO Nanosheets for Rechargeable Zinc−Air Batteries, ACS Appl. Mater. Interfaces. 2019;11:30865−30871.
DOI: 10.1021/acsami.9b08647
52. Wang XH, Wang J, Li YB, Chu K. Nitrogen-Doped NiO Nanosheet Array for Boosted Electrocatalytic N_2 Reduction, Chem. Cat. Chem. 2019;11:4529–4536.
DOI: 10.1002/cctc.201901075

53. Lin CW, Chung WC, Zhang ZD, Hsu MC. P-channel transparent thin-film transistor using physical-vapor-deposited NiO layer, Jpn. J. Appl. Phys. 2018;57:01AE01(5pp).
DOI: 10.7567/JJAP.57.01AE01
54. Davis EA, Mott,NF. Conduction in non-crystalline systems V. Conductivity, optical absorption and photoconductivity in amorphous semiconductors, Philosophical Magazine. 1970;22:0903-0922.
DOI: 10.1080/14786437008221061
55. Chopra KL, Bahlt SK. Exponential tail of the optical absorption edge of amorphous semiconductors, Thin Solid Films. 1972;I1:377-388.
DOI: 10.1016/0040- 6090(72)90063-6
56. Choudhury B, Choudhury A. Oxygen defect dependent variation of band gap, Urbach energy and luminescence property of anatase, anatase–rutile mixed phase and of rutile phases of TiO_2 nanoparticles, Physica E. 2014;56:364-371.
DOI: 10.1016/j.physe.2013.10.014
57. Akshay VR, Arun B, Mandal G, Vasundhara M. Visible range optical absorption, Urbach energy estimation and paramagnetic response in Cr-doped TiO_2 nanocrystals derived by a sol–gel method, Phys. Chem. Chem. Phys. 2019;21:12991-13004.
DOI: 10.1039/c9cp01351b
58. Klochko NP, Klepikova KS, Kopach VR, Khrypunov GS, Myagchenko YO, Melnychuk EE, et al. On Controlling the Hydrophobicity of Nanostructured Zinc-Oxide Layers Grown by Pulsed Electrodeposition, Semiconductors. 2016;50:352-363.
DOI: 10.1134/S106378261603012X
59. Anyaegbunam FNC, Augustine C. A study of optical band gap and associated urbach energy tail of chemically deposited metal oxides binary thin films, Digest Journal of Nanomaterials and Biostructures. 2018;13:847-856.
60. Biswas D, Das AS, Mondal R, Banerjee A, Dutta A, Kabi S, Roy D, Singh LS. Structural properties and electrical conductivity mechanisms of semiconducting quaternary nanocomposites: Effect of two transition metal oxides, J. Phys. Chem. 2020;144:109505(14pp).
DOI: 10.1016/j.jpcs.2020.109505
61. Sharma N, Prabakar K, Ilango S, Dash S, Tyagi AK. Optical band-gap and associated Urbach energy tails in defected AlN thin films grown by ion beam sputter deposition: Effect of assisted ion energy, Adv. Mat. Proc. 2017;2:342-346.
DOI: 10.5185/amp.2017/511
62. Hassanien AS, Akl AA. Effect of Se addition on optical and electrical properties of chalcogenide CdSSe thin films, Superlattices and Microstructures. 2016;89:153-169.
DOI: 10.1016/j.spmi.2015.10.044
63. Kozlova SG, Ryzhikov MR, Shayapov VR, Samsonenko DG. Effect of spin– phonon interactions on Urbach tails in flexible [$M_2(bdc)_2(dabco)$], Phys. Chem. Chem. Phys. 2020;22:15242-15247.
DOI: 10.1039/d0cp01944e
64. Wolf SDE, Holovsky J, Moon SJ, Lopper P, Niesen B, Ledinsky M, et al. Organometallic Halide Perovskites: Sharp Optical Absorption Edge and Its Relation to Photovoltaic Performance, J. Phys. Chem. Lett. 2014;5:1035- 1039.
DOI: 10.1021/jz500279b
65. Ishikawa R, Kato T, Anzo R, Nagatake M, Nishimura T, Tsuboi N, Miyajima S. Widegap $CH_3NH_3PbBr_3$ solar cells for optical wireless power transmission application, Appl. Phys. Lett. 2020;117:013902(5pp).
DOI: 10.1063/5.0010009
66. Siddique MN, Ahmed A, Tripathi P. Enhanced optical properties of pure and Sr doped NiO nanostructures: A comprehensive study, Optik. 2019;185:599-608.
DOI: 10.1016/j.ijleo.2019.03.150
67. Boukhari JAl, Zeidan L, Khalaf A, Awad R. Synthesis, characterization, optical and magnetic properties of pure and Mn, Fe and Zn doped NiO nanoparticles, Chem. Phys. 2019;516:116-124.
DOI: 10.1016/j.chemphys.2018.07.046

68. Maiti S, van der Laan M, Poonia D, Schall P, Kinge S, Siebbeles LDA. Emergence of new materials for exploiting highly efficient carrier multiplication in photovoltaics, Chem. Phys. Rev. 2020;1:011302.
DOI: 10.1063/5.0025748
69. Aperathitis E, Bender M, Cimalla V, Ecke G, Modreanu M. Properties of rf- sputtered indium–tin-oxynitride thin films, J. Appl. Phys. 2003;94:1258-1266.
DOI: 10.1063/1.1582368
70. Gong H, Chen X, Xu Y, Chen Y, Ren F, Liu B, Gu S, Zhang R, Ye J. Band Alignment and Interface Recombination in NiO/β-Ga_2O_3 Type-II p-n Heterojunctions, IEEE Trans. Electron Devices. 2020;67:3341-3347.
DOI: 10.1109/TED.2020.3001249
71. Abbas S, Kim J.All-metal oxide transparent photodetector for broad responses, Sensors and Actuators A. 2020;303:111835(8pp).
DOI: 10.1016/j.sna.2020.111835
72. Egbo KO, Kong M, Liu CP, Yu KM. Room temperature sputtered Cu doped $NiO_{1+\delta}$: p-type conductivity, stability of electrical properties and p-n heterojunction, J. Alloys and Compounds. 2020;835:155269(12pp).
DOI: 10.1016/j.jallcom.2020.155269
73. Lin F, Gillaspie DT, Dillon AC, Richards RM, Engtrakul C. Nitrogen-doped nickel oxide thin films for enhanced electrochromic applications, Thin Solid Films. 2013;527:26-30.
DOI: 10.1016/j.tsf.2012.12.031
74. Gagaoudakis E, Aperathitis E, Michail G, Kiriakidis G, Binas V. Sputtered VO_2 coatings on commercial glass substrates for smart glazing applications, Solar Energy Materials & Solar Cells. 2021;220:110845(9pp).
DOI: 10.1016/j.solmat.2020.110845
75. Sze SM. Physics of Semiconductor Devices, 2nd ed., John Wiley and Sons Ltd1981, 2nd edition. Wiley, New York; 1981.
ISBN-13: 978-0471098379.
76. Cheung SK, Cheung NW. Extraction of Schottky diode parameters from forward current-voltage characteristics, Appl. Phys. Lett. 1986;49:85-87.
DOI: 10.1063/1.97359
77. Robinson GY. Schottky Diodes and Ohmic Contacts for the III-V Semiconductors, in Physics and Chemistry of III -V Compound Semiconductor Interfaces. Ed. C.W. Wilmsen, Plenum Press; 1985.
DOI: 10.1007/978-1-4684-4835-1
78. Schroder DK. Semiconductor Material and Device Characterization, 3rd Edition, John Wiley & Sons; 2006.
ISBN-13: 978-0-471-73906-7
79. Al-Ahmadi NA, Ebrahim FA, Al-Jawhari HA, Mari RH, Henini M. Impact of doping on the performance of p-type Be-doped $Al_{0.29}Ga_{0.71}As$ Schottky diodes, Modern Electronic Materials. 2017;3:66-71.
DOI: 10.1016/j.moem.2017.06.001
80. Hasan MR, Xie T, Barron SC, Liu G, Nguyen NV, Motayed A, Rao MV, Debnath R. Self-powered p-NiO/n-ZnO heterojunction ultraviolet photodetectors fabricated on plastic substrates, APL Mater. 2015;3:106101(7pp).
DOI: 10.1063/1.4932194

Biography of author(s)

Chrysa Aivalioti
Department of Materials Science and Technology, University of Crete, P.O. Box 2208, 71003, Heraklion, Crete, Greece.
Microelectronics Research Group, Institute of Electronic Structure and Laser, Foundation for Research and Technology (FORTH-Hellas), P.O. Box 1385, Heraklion, Greece.

Author Bio available in this link:https://www.bookpi.org/wp-content/uploads/2022/01/Chrysa-Aivalioti_Bio.pdf

Alexandros Papadakis
Department of Physics, University of Crete, P.O. Box 2208, 71003, Heraklion, Crete, Greece.

He was born and raised in Heraklion, Crete, Greece. He was always keen on questioning and seeking to learn new information about how things around us, and in nature in general. He is extremely interested in the Semiconductors' Physics and in their microelectronic and optoelectronic applications. He also find highly intriguing 'green' projects such as Solar Cells, Transparent Solar cells, Polymer Solar Cells, etc. he is also interested in the physics and chemistry of materials. He is a Graduate of the 4th High school of Heraklion , Crete, Greece. He completed his BSc in Physics, University Of Crete , Completed 2 Computer Labs (Physics Department, University of Crete), Electromagnetism Laboratory (Physics Department, University of Crete), Optics Laboratory (Physics Department, University of Crete), Advanced Physics Laboratory (Physics Department, University of Crete), Physics of Semiconductors Laboratory (Physics Department, University of Crete), Electronic Components Laboratory (Physics Department, University of Crete), and Lasers and Modern Optics Laboratory(I.E.S.L Crete, Greece).

Emmanouil Manidakis
Department of Materials Science and Technology, University of Crete, P.O. Box 2208, 71003, Heraklion, Crete, Greece.
Microelectronics Research Group, Institute of Electronic Structure and Laser, Foundation for Research and Technology (FORTH-Hellas), P.O. Box 1385, Heraklion, Greece.

Author Bio available in this link:https://www.bookpi.org/wp-content/uploads/2022/01/Emmanouil-Manidakis_Bio.pdf

Maria Kayambaki
Microelectronics Research Group, Institute of Electronic Structure and Laser, Foundation for Research and Technology (FORTH-Hellas), P.O. Box 1385, Heraklion, Greece.

She obtained her B.Sc degree in Physics from the University of Crete, Greece in 1992. Since the March of 1992, she is a research assistant at Microelectronics Research group of Institute of Electronic structure and Laser (Foundation for Research and Technology-Hellas), responsible for Electrical and Electrochemical characterization of novel semiconductors and semiconductor devices, such as III-nitrides, SiC and GaAs. She is specialized in the techniques of Deep Level Transient Spectroscopy (DLTS), Capacitance-Voltage measurements during Electrochemical etching (ECV), Current-Voltage (I-V) and Capacitance-Voltage (C-V) measurements on high frequency (HEMTs) and high power (JFETs) transistors. She has published and participated in more than 50 publications in international journals and conferences.

Maria Androulidaki
Microelectronics Research Group, Institute of Electronic Structure and Laser, Foundation for Research and Technology (FORTH-Hellas), P.O. Box 1385, Heraklion, Greece.

She received a degree in Physics and a postgraduate diploma (Ms.c) in Solid State Physics from the University of Crete. She works with an indefinite employment relationship in the Microelectronics Team of the Institute of Electronic Structure and Laser of FORTH, as a research technician. Her research activity includes the optical characterization of semiconductors and other materials with the technique of photoluminescence (PL), micro-PL, Transmittance (T) and reflectance (R), micro-Raman and infrared absorption (FTIR) measurements and the characterization of optoelectronic devices , such as led structures, photovoltaics etc. She participates in research programs and in education and supervision of students in the laboratory. She has collaborated with institutions in Greece. She has over 100 publications and a corresponding Hirsch rate of 18 (SCOPUS database, September 2021). ORCID ID: 0000-0002-6772-8851.

Katerina Tsagaraki
Microelectronics Research Group, Institute of Electronic Structure and Laser, Foundation for Research and Technology (FORTH-Hellas), P.O. Box 1385, Heraklion, Greece.

Author Bio available in this link:https://www.bookpi.org/wp-content/uploads/2022/01/Katerina-Tsagaraki-Bio.pdf

Nikolaos T. Pelekanos
Department of Materials Science and Technology, University of Crete, P.O. Box 2208, 71003, Heraklion, Crete, Greece.
Microelectronics Research Group, Institute of Electronic Structure and Laser, Foundation for Research and Technology (FORTH-Hellas), P.O. Box 1385, Heraklion, Greece.

He obtained his Ph.D in 1991 from Brown University, USA, on the optical properties of two-dimensional II-VI compound semiconductors. After a number of post-doctoral stays in various European labs, including the France Telecom Research Center in Lannion and the Max-Planck Institute in Stuttgart, he joined the Semiconductor Physics Laboratory at CEA-Grenoble from 1995 until 2001. Next, he joined the Microelectronics Research group at FORTH in 2001 and the Materials Science and Technology Department of the University of Crete in 2003. His main research theme is the demonstration of novel semiconductor nanophotonic devices, including quantum dot-based high temperature sources of single and entangled photons, polariton lasers and parametric scattering amplifiers at room temperature, and next-generation solar cells based on hybrid halide perovskites and III-V semiconductor nanostructures. He has coordinated/participated in numerous European, bilateral and national projects. He has obtained the "Solar Innovation 2010" award for his proposal on third-generation low-dimensional semiconductor solar cells, and more recentlya Chair of Excellence LANEF, funded by the French government, for a project entitled “Nanowire Innovative Solar Cells”. He has published over 250 publications in refereed journals and conference proceedings and holds 6 technical patents.

Mircea Modreanu
Tyndall National Institute-University College Cork, Lee Maltings, Dyke Parade, Cork, T12 R5CP, Ireland.

He received M.Sc. (1993) and Ph.D. (2002) in Condensed Matter physics from the Faculty of Physics, University of Bucharest, Italy. From 1993 to 2002 he was working as a Senior Researcher in IMT-Bucharest, Romania. In 2002 he has joined Tyndall National Institute-University College Cork, Ireland working as Principal Investigator in the Micro & Nano Systems Centre. He has received short-term professor fellowships from INPG-PHELMA, France, and from JSPS, Japan. His main expertise comprises the nonmaterial development for micro-nanoelectronics, nanophotonics, and RF/microwave/millimeter-wave/ systems for targeted wireless/energy-harvesting applications. In addition, he has extensive expertise in many areas of optical spectroscopies. In the last two decades, he has been involved in several EU-funded projects, and currently, his research activity is supported by European Innovation Council. He has co-authored more than 140 papers in ISI-ranked journals and conferences. He was organized several international conferences in Europe and Japan in the area of optical and x-ray metrologies for advanced materials and nanoscale devices.

Gabriel Crăciun
National Institute for Research and Development in Microtechnologies -IMT, Bucharest, Romania.

He is a Scientific Researcher III, Physicist. He has Expertise on Semiconductor technology clean room techniques and processes, PVD (Physical Vapor Deposition) techniques - particularly deposition of thin films by e-beam induced evaporation, SEM (Scanning Electron Microscopy) sample imagistic investigation technique; investigations and compositional analysis of materials by EDX (Energy-dispersive X-ray spectroscopy) technique. He Authored and co-authored 19 papers published in international journals and 34 papers presented at international conferences and published in conference proceedings.

Cosmin Romanitan
National Institute for Research and Development in Microtechnologies -IMT, Bucharest, Romania.

He received PhD in physics from the Department of Solid-State Physics, University of Bucharest in 2019. His research activity expanded in the frame of 26 research projects focusing on investigation of microstructural properties nanomaterials (e.g. lattice parameters, size of the crystalline domains, constituent phases, preferential orientation, thickness, roughness, density, type and number of structural defects in epitaxial layers)in connection with their applicative potential for charge storage devices, electrochromic devices, sensors or photodetectors. For instance, he successfully determined the density of edge and screw threading dislocations in gallium based thin films, such as gallium nitride or gallium arsenide doped with Bi by means of high-resolution X-ray diffraction. As for the porous layers with high specific surface area he revealed both the strain formation and the pores' morphology in correlation with their capacity of storing charges, as well as he proposed a non-destructive formalism to reveal the porosity gradient using small angle X-ray scattering and/or high-resolution configurations. Also, he investigated the Li+ intercalation processes in V2O5 and their role in electrochromic and charge storage processes and further,it was established the relationship between the texture coefficient along (001) direction and the inserted charge in orthorhombic α-V2O5 with applications in electrochromic and charge storage devices. He has Number of ISI papers: 54; Number of citations: 245; h-index = 8 (according to WoS).

Elias Aperathitis
Microelectronics Research Group, Institute of Electronic Structure and Laser, Foundation for Research and Technology (FORTH-Hellas), P.O. Box 1385, Heraklion, Greece.

He completed M.Sc. in "Physics and Technology of Amorphous Materials", 1984, Univ. of Dundee, Scotland; Ph.D. in "Thin Film Solar Cells", 1989, Univ. of Hull, England. Since 1991, he is Principal (Application) Scientist at Microelectronics Research Group (MRG) of Institute of Electronic Structure & Laser (IESL) of Foundation for Research and Technology-Hellas (FORTH), Crete, Greece. In January 2017 he was appointed Safety Manager for MRG/IESL. He has conducted research in the fabrication/processing and characterization of semiconductors (III-V, III-N & oxides) materials/devices and he has participated as IESL/FORTH Key Researcher for many European, National as well as Bilateral research projects on optoelectronics. He is currently involved in the development of novel thin film oxide/nitride/oxynitride-based materials and devices for transparent microelectronics, optoelectronics and energy efficient buildings. He is program and steering committee member in several international conferences related to materials and devices in the areas of electronics and photonics. He serves regularly as reviewer in scientific journals. He has 78 publications, h-index 17 and 774 citations. IDs: OrcidID: 0000-0002-2800-7509, ResearcherID: O-2973-2013, Scopus Author ID: 6701842312.

© Copyright (2022): Author(s). The licensee is the publisher (B P International).

DISCLAIMER
This chapter is an extended version of the article published by the same author(s) in the following journal.
Electronics, 10: 988, 2021.